Infectious Disease Modelling 10 (2025) 1055–1092

Contents lists available at ScienceDirect

Infectious Disease Modelling

journal homepage: www.keaipublishing.com/idm

Modeling the impact of hospitalization-induced behavioral changes on the spread of COVID-19 in New York City

Alice Oveson [a], Michelle Girvan [b], Abba B. Gumel [a, c, d, *]

[a] Department of Mathematics, University of Maryland, College Park, MD, 20742, USA
[b] Department of Physics, University of Maryland, College Park, MD, 20742, USA
[c] Institute for Health Computing, University of Maryland, North Bethesda, Maryland, 20852, USA
[d] Department of Mathematics and Applied Mathematics, University of Pretoria, Pretoria, 0002, South Africa

ARTICLE INFO

Article history:
Received 21 January 2025
Received in revised form 1 May 2025
Accepted 2 May 2025
Available online 27 May 2025
Handling Editor: Dr Yijun Lou

Keywords:
Behavioral-epidemiology model
COVID-19
Equilibria
Influence dynamics

ABSTRACT

The COVID-19 pandemic, caused by SARS-CoV-2, highlighted heterogeneities in human behavior and attitudes of individuals with respect to adherence or lack thereof to public health-mandated intervention and mitigation measures. This study is based on using mathematical modeling approaches, backed by data analytics and computation, to theoretically assess the impact of human behavioral changes on the trajectory, burden, and control of the COVID-19 pandemic during the first two waves in New York City. A novel behavior-epidemiology model, which considers n heterogeneous behavioral groups based on level of risk tolerance and distinguishes behavioral changes by social and disease-related motivations (such as peer-influence and fear of disease-related hospitalizations), is developed. In addition to rigorously analyzing the basic qualitative features of this model, a special case is considered where the total population is stratified into two groups: risk-averse (Group 1) and risk-tolerant (Group 2). The 2-group model was calibrated and validated using daily hospitalization data for New York City during the first wave, and the calibrated model was used to predict the data for the second wave. The 2-group model predicts the daily hospitalizations during the second wave almost perfectly, compared to the version without behavioral considerations, which fails to accurately predict the second wave. This suggests that epidemic models of the COVID-19 pandemic that do not explicitly account for heterogeneities in human behavior may fail to accurately predict the trajectory and burden of the pandemic in a population. Numerical simulations of the calibrated 2-group behavior model showed that while the dynamics of the COVID-19 pandemic during the first wave was largely influenced by the behavior of the risk-tolerant (Group 2) individuals, the dynamics during the second wave was influenced by the behavior of individuals in both groups. It was also shown that disease-motivated behavioral changes (i.e., behavior changes due to the level of COVID-19 hospitalizations in the community) had greater influence in significantly reducing COVID-19 morbidity and mortality than behavior changes due to the level of peer or social influence or pressure. Finally, it is shown that the initial proportion of members in the community that are risk-averse (i.e., the proportion of individuals in Group 1 at the beginning of the pandemic) and the early and effective implementation of non-pharmaceutical interventions have major impacts in reducing the size and burden of the pandemic (particularly the total COVID-19 mortality in New York City during the second wave).

* Corresponding author. Department of Mathematics, University of Maryland, College Park, MD, 20742, USA.
E-mail address: agumel@umd.edu (A.B. Gumel).
Peer review under the responsibility of KeAi Communications Co., Ltd.

https://doi.org/10.1016/j.idm.2025.05.001

1. Introduction

The novel pneumonia-like illness that emerged in Wuhan, China in December 2019, coined the 2019 coronavirus (COVID-19) and caused by SARS-CoV-2, spread rapidly within China and to other parts of the world, prompting the World Health Organization to declare a global pandemic of COVID-19 in March 2020. With over 775 million cases and over 7 million deaths globally (World Health Organization, 2023), the toll of COVID-19 is long-lasting. It caused many healthcare workers to leave the field, leading to long-term staffing shortages (ASPE Office of Health Policy, 2022; United States Bureau of Labor Statistics, 2024) and downturns in the global economy (Garad et al., 2021; Naseer et al., 2022; Walmsley et al., 2023), education quality (Di Pietro, 2023; Tang, 2022), and mental health across the world (Ferwana & Varshney, 2024; Panchal et al., 2023). Additionally, it resulted in dramatic increases in the level of political polarization, inequity and disparity in access to healthcare (Gmunder et al., 2021), the spread of misinformation and disinformation (Ferrara et al., 2020; Mian & Khan, 2020), anti-vaccination movements (Altman et al., 2023; Carpiano et al., 2023), distrust of governments and public health agencies (Di Marco et al., 2021; Scandurra et al., 2023; Zhai & Han, 2023), and incidence of domestic violence (Boserup et al., 2020; Bradbury-Jones & Ishlam, 2020; Sediri et al., 2020). Four years into the pandemic (November 2024), nearly 1, 000 people die each week globally of COVID-19 related causes, despite the widespread availability of life-saving vaccines (World Health Organization, 2023).

The behavioral response to the COVID-19 pandemic in the US and globally was highly heterogeneous (Fan et al., 2020; Shin et al., 2021), largely due to individual-level differences, such as heterogeneities with respect to the quality of the pandemic-related information received (Uscinski, 2022), economic status and amount of savings (Stoler, 2022), trust of government and health agencies (Stoler, 2022), and social pressures (Yang et al., 2022). This behavioral heterogeneity played a major role in shaping the trajectory and burden of the pandemic (Arthur et al., 2021; Berestycki et al., 2021; LeJeune et al., 2024). Numerous modeling types, including compartmental (Arthur et al., 2021; Berestycki et al., 2023; Del Valle et al., 2013; Eksin et al., 2019; Espinoza et al., 2021, Espinoza et al., 2022; He et al., 2013; LeJeune et al., 2024; Nguyen et al., 2024; Ochab et al., 2023; Pant et al., 2024; Pisaneschi et al., 2024; Saad-Roy & Traulsen, 2023; Sharbayta et al., 2022; Weitz et al., 2020), agent-based (Chen et al., 2024; Del Valle et al., 2013; Kitson et al., 2023; Martin-Lapoirie et al., 2023; Yang et al., 2022), and network (Chen et al., 2024; Eksin et al., 2017; Funk & Jansen, 2013; Kitson et al., 2023; Qiu et al., 2022; Waites, 2022), have been used to gain insight and understanding into the role of human behavior changes (or heterogeneities) on the spread and control of the COVID-19 pandemic. These models typically assume that individual disease-related behavior change, such as adherence or non-adherence to public health interventions, reducing contacts, etc., is motivated by a combination of disease-related metrics (such as the level of disease prevalence and intervention fatigue in their local community or population) (Nguyen et al., 2024; Pant et al., 2024; Saad-Roy & Traulsen, 2023; Sharbayta et al., 2022), peer pressure or influence (Martin-Lapoirie et al., 2023; Pant et al., 2024; Qiu et al., 2022; Yang et al., 2022), and other costs associated with adoption of disease-related precautionary behaviors). For example, the compartmental model developed by Pisaneschi et al. (Pisaneschi et al., 2024) accounts for average daily wages, assuming that a lower wage will force individuals to abandon disease-related precautionary behaviors. These behavioral heterogeneities and changes are typically modeled by incorporating an adaptive transmission rate that is dependent on disease prevalence (Eksin et al., 2019; Espinoza et al., 2022; LeJeune et al., 2024) or by stratifying the members of the population into various mutually exclusive compartments based on their disease-related behavioral choices or attitudes (Espinoza et al., 2021, Espinoza et al., 2022; Pant et al., 2024; Saad-Roy & Traulsen, 2023; Yang et al., 2022) (i.e., a higher transmission rate is assumed for the individuals in the risk-taking compartment, compared to those in the compartment for risk-averse individuals).

Prior modeling studies showed that behavioral heterogeneities and changes occur at a group level (i.e., the whole population becomes more or less cautious, in comparison to its behavioral choices before the onset of the disease or during an earlier phase of its progression) (Espinoza et al., 2022; LeJeune et al., 2024) and at an individual level (i.e., certain individuals will alter their past behavior or attitude with respect to the disease, despite the trends or choices made by the general population) (Pant et al., 2024; Qiu et al., 2022; Yang et al., 2022), and that both types of behavior changes strongly influence the trajectory and burden of the pandemic (Bansal et al., 2007). For example, Espinoza et al. (Espinoza et al., 2022) used a game-theoretic compartmental model (with a utility function that influences the contact rate within the population), which stratifies the susceptible, exposed, and asymptomatic portions of the population based on compliance or lack thereof to

interventions, and showed that heterogeneous responses based on perceived risk (calculated using only the number of symptomatically infectious individuals) can increase the final size of the COVID-19 pandemic. Furthermore, several other modeling studies confirmed that asymptomatic transmission was a major driver of the COVID-19 pandemic (Espinoza et al., 2021; Moghadas et al., 2020; Ngonghala, Iboi, & Gumel, 2020; Nishiura et al., 2020; Pant et al., 2024), resulting in large disparity between true and perceived disease prevalence (which changed people's behavior or attitude towards the pandemic (Espinoza et al., 2021)). Specifically, Pant et al. (Pant et al., 2024) showed a strong correlation between the proportion of newly infected individuals who become asymptomatically infectious and decreases in positive behavior changes with respect to public health control and mitigation measures. These studies clearly show that the effect of human behavior changes during the COVID-19 pandemic can be incorporated into epidemiological models using measurable and publicly available health metrics (such as the number of new confirmed/symptomatic cases, hospitalizations, and disease-induced mortality) and sociological metrics (e.g., intervention fatigue) (Pant et al., 2024).

The objective of the current study is to assess the population-level impact of behavioral changes, with respect to levels of hospitalization, on the transmission dynamics and control of the COVID-19 pandemic in New York City. To achieve this objective, a multi-group compartmental model is developed, which subdivides the total population into n heterogeneous groups that differ based on their behavior and/or attitude towards the disease. Specifically, the model takes into account how adverse group members are to acquiring (if they are not infected or unaware of their infection) or transmitting (if they are infected and aware of their infection) the disease. The model, which consists of a deterministic system of nonlinear differential equations, will be parameterized using observed COVID-19 hospitalization data in New York City during the first wave of the pandemic. Furthermore, group-level behavioral change will be accounted for by incorporating a time-varying parameter that accounts for the relative reduction in individual contact rates. This parameter will have a nonlinear dependence on perceived risk of acquisition and transmission of infection, measured by the proportion of hospitalized individuals in the community (New York City). The paper is organized as follows. The model (with n heterogeneous behavioral groups), tagged *the behavior model*, is formulated in Section 2. For the special case with $n = 2$ behavioral groups, the stability of the disease-free equilibria is analyzed in Section 3.1. The model with $n = 2$ behavioral groups is fitted and cross-validated with observed data for the first wave of the COVID-19 pandemic in New York City in Section 3.2. To assess the impact of behavior on accurately capturing the correct trajectory and burden of the pandemic, the behavior-free equivalent of the model is also fitted and cross-validated for comparison purposes (specifically, the objective is to determine which of the two models, behavior vs. behavior-free, fits and cross-validates the observed data more accurately). Global parameter sensitivity analysis and numerical simulations of the behavior model are reported in Sections 3.4 and 3.5, respectively. Discussion and concluding remarks are presented in Section 4.

2. Formulation of the behavior model

The focus is to develop a mechanistic model for assessing the population-level impact of hospitalization-induced and peer pressure–induced behavior changes on the transmission dynamics of the COVID-19 pandemic in New York City during the first wave (which ran from late February 2020 to late July 2020 (Centers for Disease Control, 2023). The model is formulated by subdividing the total population at time t, denoted by $N(t)$, into n heterogeneous behavioral groups based on their perceived risk (of acquisition/transmission of infection) and their resulting behavior choices with respect to the risk. Group 1 represents individuals in the community who consistently adopt the most risk-averse behaviors against the acquisition or transmission of the disease by consistently and strictly adhering to public health intervention and mitigation measures. Similarly, Groups 2 through n represent sub-groups within the community who adopt more risk-taking behaviors, with Group n representing the individuals in the community who adopt the most risk tolerant behaviors (Nguyen et al., 2024). Each of the n heterogeneous behavioral groups is further subdivided into the mutually exclusive compartments of susceptible ($S_i(t)$), exposed ($E_i(t)$), asymptomatically infectious ($I_{a,i}(t)$), symptomatically infectious ($I_{s,i}(t)$), hospitalized ($I_{h,i}(t)$) and recovered ($R_i(t)$) individuals (with $i = 1, 2, \ldots, n$) so that

$$N_i(t) = S_i(t) + E_i(t) + I_{a,i}(t) + I_{s,i}(t) + I_{h,i}(t) + R_i(t).$$

The equations for the rate of change of each of the aforementioned epidemiological compartments (for each of the n behavioral sub-groups) are given by the following deterministic system of nonlinear differential equations (where a dot represents differentiation with respect to time t, and $i = 1, 2, \ldots, n$):

$$
\begin{aligned}
\dot{S}_i(t) &= \xi R_i(t) - \theta_l\left[\frac{c_i^A(t)S_i(t)}{N(t)}\right]\sum_{j=1}^{n} c_j^A(t)\left[\beta_a I_{a,j}(t) + \beta_i I_{s,j}(t) + \beta_h I_{h,j}(t)\right] \\
&\quad + \frac{S_{i-1}(t)}{N(t)}\sum_{j=i}^{n} c^B_{j(i-1)}N_j(t) + \frac{S_{i+1}(t)}{N(t)}\sum_{j=1}^{i} c^B_{j(i+1)}N_j(t) - \frac{S_i(t)}{N(t)}\sum_{j=1 j\neq i}^{n} c^B_{ji}N_j(t), \\
\dot{E}_i(t) &= \theta_l\left[\frac{c_i^A(t)S_i(t)}{N(t)}\right]\sum_{j=1}^{n} c_j^A(t)\left[\beta_a I_{a,j}(t) + \beta_i I_{s,j}(t) + \beta_h I_{h,j}(t)\right] - \sigma_e E_i(t) \\
&\quad + \frac{E_{i-1}(t)}{N(t)}\sum_{j=i}^{n} c^B_{j(i-1)}N_j(t) + \frac{E_{i+1}(t)}{N(t)}\sum_{j=1}^{i} c^B_{j(i+1)}N_j(t) - \frac{E_i(t)}{N(t)}\sum_{j=1 j\neq i}^{n} c^B_{ji}N_j(t), \\
\dot{I}_{a,i}(t) &= (1-r)\sigma_e E_i(t) - \gamma_a I_{a,i}(t) \\
&\quad + \frac{I_{a,i-1}(t)}{N(t)}\sum_{j=i}^{n} c^B_{j(i-1)}N_j(t) + \frac{I_{a,i+1}(t)}{N(t)}\sum_{j=1}^{i} c^B_{j(i+1)}N_j(t) - \frac{I_{a,i}(t)}{N(t)}\sum_{j=1 j\neq i}^{n} c^B_{ji}N_j(t), \\
\dot{I}_{s,i}(t) &= r\sigma_e E_i(t) - \sigma_i I_{s,i}(t) \\
&\quad + \frac{I_{s,i-1}(t)}{N(t)}\sum_{j=i}^{n} c^B_{j(i-1)}N_j(t) + \frac{I_{s,i+1}(t)}{N(t)}\sum_{j=1}^{i} c^B_{j(i+1)}N_j(t) - \frac{I_{s,i}(t)}{N(t)}\sum_{j=1 j\neq i}^{n} c^B_{ji}N_j(t), \\
\dot{I}_{h,i}(t) &= q\sigma_i I_{s,i}(t) - (\gamma_h + \delta_h)I_{h,i}(t) \\
&\quad + \frac{I_{h,i-1}(t)}{N(t)}\sum_{j=i}^{n} c^B_{j(i-1)}N_j(t) + \frac{I_{h,i+1}(t)}{N(t)}\sum_{j=1}^{i} c^B_{j(i+1)}N_j(t) - \frac{I_{h,i}(t)}{N(t)}\sum_{j=1 j\neq i}^{n} c^B_{ji}N_j(t), \\
\dot{R}_i(t) &= \gamma_a I_{a,i}(t) + (1-q)\sigma_i I_{s,i}(t) + \gamma_h I_{h,i}(t) - \xi R_i(t) \\
&\quad + \frac{R_{i-1}(t)}{N(t)}\sum_{j=i}^{n} c^B_{j(i-1)}N_j(t) + \frac{R_{i+1}(t)}{N(t)}\sum_{j=1}^{i} c^B_{j(i+1)}N_j(t) - \frac{R_i(t)}{N(t)}\sum_{j=1 j\neq i}^{n} c^B_{ji}N_j(t).
\end{aligned}
\tag{2.1}
$$

A flow diagram of the heterogeneous n-group behavior model (2.1) is depicted in Fig. 1, and the state variables and parameters of the model are described in Tables 1 and 2, respectively.

In model (2.1), susceptible individuals in Behavioral Group i (i.e., S_i) acquire COVID-19 infection at a rate, λ (known as the *force of infection*), given by (with $i = 1, 2, \ldots, n$):

$$
\lambda = (\theta_l)\left[\frac{c_i^A(t)S_i(t)}{N(t)}\right]\sum_{j=1}^{n} c_j^A(t)\left[\beta_a I_{a,j}(t) + \beta_i I_{s,j}(t) + \beta_h I_{h,j}(t)\right],
$$

where $0 < c_i^A(t) \leq 1$ is a modification parameter accounting for the reduction in risky behavior by individuals in Group i due to the size of the proportion of individuals hospitalized due to COVID-19 in the community (the corresponding modification parameter for individuals in Group j, with $j = 1, 2, \ldots, n$ and $j \neq i$, is $c_j^A(t)$. Specifically, the modification parameter $c_i^A(t)$ is defined as:

$$
c_i^A(t) = e^{-a_i I_h(t)/N(t)},\ i = 1, 2, \ldots, n, \tag{2.2}
$$

where $I_h(t) = \sum_{i=1}^{n} I_{h,i}(t)$ is the number of individuals in the community who are hospitalized with COVID-19 at time t, and the exponent $a_i \gg 1$ is a measure of hospitalization-induced positive behavioral changes by individuals in Group i. It is assumed that individuals in the more cautious behavioral groups (i.e., individuals in Group i, where i is relatively low, in comparison to n) will positively change their behaviors more readily than those in the less cautious behavioral groups (i.e., those in Group i

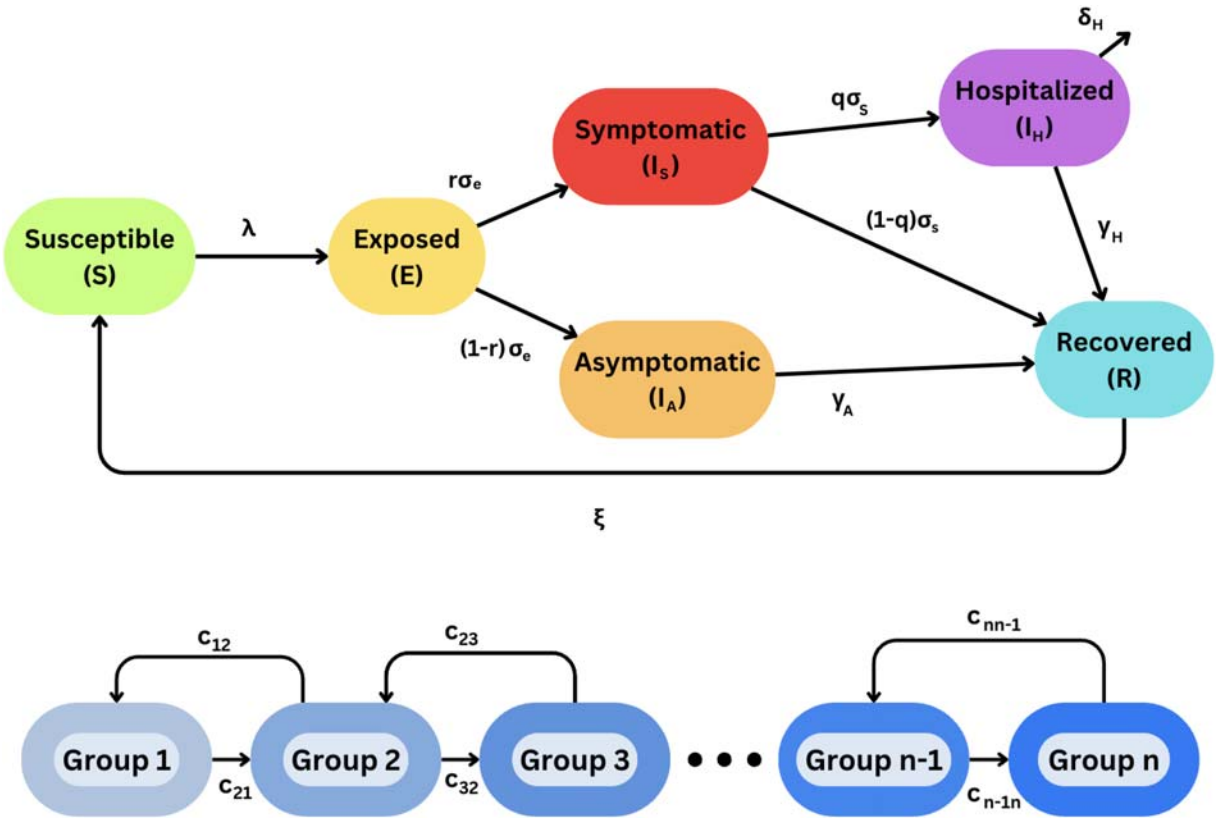

Fig. 1. Flow diagram of the heterogeneous n-group behavior model (2.1), illustrating the disease dynamics (top panel) and the influence dynamics with n behavioral groups (bottom panel).

Table 1
Description of the state variables of the heterogeneous n-group behavior model (2.1).

State variable	Description
S_i	Population of susceptible individuals in Behavioral Group i
E_i	Population of exposed individuals in Behavioral Group i
$I_{a,i}$	Population of asymptomatically infectious individuals in Behavioral Group i
$I_{s,i}$	Population of symptomatically infectious individuals in Behavioral Group i
$I_{h,i}$	Population of hospitalized individuals in Behavioral Group i
R_i	Population of recovered individuals in Behavioral Group i

with i close enough to n). Fig. 2 shows that a higher value of a_i results in a larger reduction in the contact rate by individuals in Behavioral Group i (and, as a result, the force of infection) as a function of the proportion of individuals hospitalized in the community $I_h(t)/N(t)$.

The parameter θ_l ($0 \leq \theta_l < 1$) accounts for the effectiveness of government-mandated community lockdown (and other non-pharmaceutical intervention measures) implemented to prevent the acquisition and transmission of COVID-19 (Ngonghala, Iboi, Eikenberry, et al., 2020). When there are no government-mandated lockdowns in place, $\theta_l = 1$, as this does not reduce the force of infection. As government-mandated lockdowns are put in place and become more strict, the value of θ_l decreases. The parameters β_a, β_i and β_h represent, respectively, the maximum infection rate for infectious individuals in the asymptomatic, symptomatic and hospitalized compartments.

Recovered individuals lose their infection-acquired (natural) immunity, and revert to the susceptible class, at a rate ξ. Exposed individuals develop clinical symptoms of COVID-19 at a rate $r\sigma_e$ (where $0 < r < 1$ is the proportion of exposed individuals who develop clinical symptoms of the disease at the end of the exposed period) or become asymptomatically infectious at a rate $(1-r)\sigma_e$ (where $1-r$ is the remaining proportion of exposed individuals who become asymptomatic at the end of the exposed period). Symptomatically infectious individuals are hospitalized at a rate $q\sigma_i$ (where $0 < q < 1$ is the proportion of symptomatically infectious individuals who are hospitalized) or recover at a rate $(1-q)\sigma_i$.

Table 2
Description of the parameters of the n-group behavior model (2.1).

Parameter ($i = 1, 2, \ldots, n$)	**Description ($i = 1, 2, \ldots, n$)**
ξ	Rate of loss of natural immunity
a_i	Modification parameter for hospitalization-induced behavioral change for individuals in Group i
$0 < (1 - c_i^A(t)) \leq 1$	A measure for the relative reduction in contact rate by individuals in Behavioral Group i due to the level of disease-related hospitalization in the community
c_{ij}^B	Rate at which individuals in Group i influence those in Group j to transition to a group closer to i (i.e., $j-1$ if $i<j$ or $j+1$ if $i>j$)
$0 < \theta_l \leq 1$	A measure for the efficacy of the government-mandated community lockdown (and other non-pharmaceutical intervention measures)
β_a	Maximum effective contact rate for asymptomatic infectious individuals
β_s	Maximum effective contact rate for symptomatic infectious individuals
β_h	Maximum effective contact rate for hospitalized individuals
σ_e	Rate of progression of exposed individuals to asymptomatic or symptomatic infectious compartment
r	Proportion of exposed individuals who become symptomatic at the end of the exposed period
$1 - r$	Proportion of exposed individuals who become asymptomatic at the end of the exposed period
σ_i	Rate at which symptomatic individuals leave the symptomatic class
q	Proportion of symptomatic individuals who are hospitalized
$1 - q$	Proportion of symptomatic individuals who recover without hospitalization
γ_a	Recovery rate for asymptomatic infectious individuals
γ_h	Recovery rate for hospitalized individuals
δ_h	Disease-induced mortality rate for hospitalized individuals

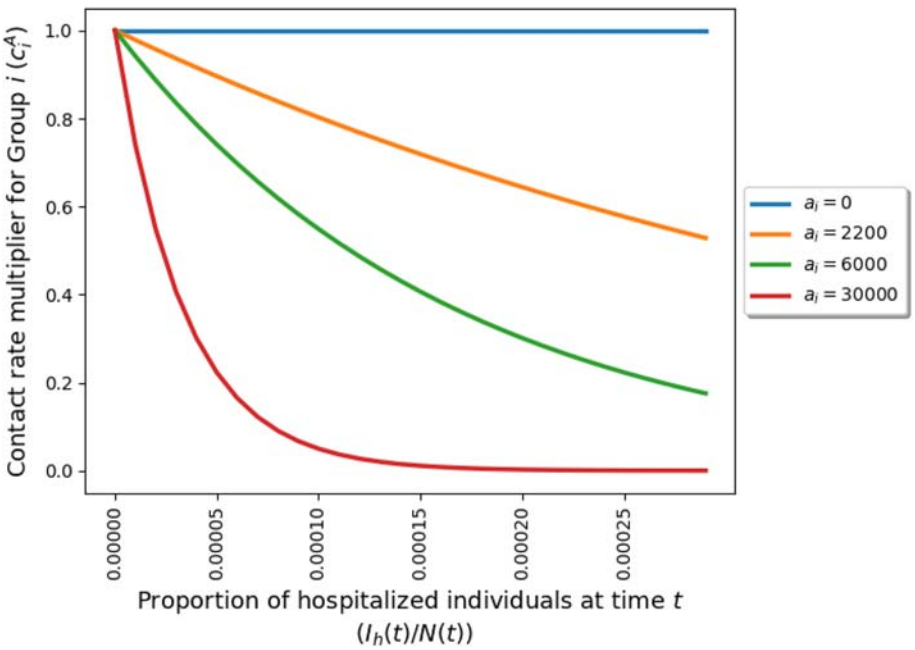

Fig. 2. Profile of the effective contact rate modification parameter $(c_i^A(t))$, as a function of the proportion of the hospitalized population $(I_h(t)/N(t))$, for various values of a_i (the modification parameter for the hospitalization-induced behavior change by individuals in Group i).

Asymptomatically infectious and hospitalized individuals recover at rates γ_a and γ_h, respectively. Hospitalized individuals suffer disease-induced mortality at a rate δ_h (it is assumed that only hospitalized infectious individuals suffer disease-related mortality, which is not a perfect assumption but is predominantly the case (Pathak et al., 2021)). Influence dynamics (where individuals in Behavioral Group i exert some degree of influence over individuals in another Behavioral Group j) are modeled using the *influence-motivated behavioral change* parameter, c_{ij}^B. Specifically, the parameter c_{ij}^B accounts for individual behavioral change in Group j with respect to public health interventions and risk-taking behavior, meaning individuals in Group j who switch behavioral groups as they are influenced by individuals in Behavioral Group i. This parameter is multiplied by the total proportion of individuals in Behavioral Group i, $(N_i(t)/N(t))$ meaning the power Behavioral Group i has to change the behavior of others is proportional to its size. Exerted influence c_{ij}^B results in a proportion of individuals in Group j changing their behavioral group and moving one group closer to Group i, going to either Group $j+1$ if $i>j$, or Group $j-1$ if $i<j$. This process is illustrated in the bottom panel of Fig. 1.

The main assumptions made in the formulation of the n-group behavior model (2.1) include:

(a) The population is closed, large, and well-mixed (i.e., homogeneous mixing between the various behavioral groups).
(b) Since the focus of this study is to model the dynamics of the COVID-19 pandemic during the first wave, no demographic (birth and natural death) processes are assumed. In other words, it is assumed that the timescale of the disease is shorter than the demographic timescale (Gumel, Iboi, Ngonghala, & Elbasha, 2021; Hethcote, 2000; Kermack & McKendrick, 1927; Martecheva, 2015)). The consequence of this assumption is that an epidemic, rather than an endemic, model will be used (Hethcote, 2000).
(c) Changes in risk-taking behaviors are induced either by (1) the level of disease burden in the community (measured by the proportion of individuals in the community hospitalized due to COVID-19 infection) or by (2) peer pressure, defined in terms of a linear function of behavioral group size. That is, larger size groups will exert more pressure than groups of smaller size. (Yang et al., 2022).
(d) Individuals currently in Behavioral Group i can only transition to the nearest behavioral groups ($i-1$ or $i+1$). This is to account for the assumption that individuals do not typically drastically change their risk-tolerance behavior over short time periods (Verplanken & Orbell, 2022).
(e) Only individuals in the hospitalized compartments ($I_{h,i}(t)$; for $i = 1, 2, \ldots, n$) can die of COVID-19 (i.e., it is assumed that individuals in other infectious compartments do not die of COVID-19, until they are hospitalized). This assumption can be justified by noting that provisional death counts from the CDC estimate that the number of COVID-19-related deaths that occurred at home was small relative to the number of COVID-19-related deaths in hospitals or other healthcare settings during the first two waves (Centers for Disease Control and Prevention, 2023).

Since the behavior model (2.1) monitors the temporal dynamics of human populations, all its parameters and state variables are non-negative for all time t. Furthermore, the model is an extension of numerous other compartmental models for the COVID-19 pandemic that incorporate human behavior changes, such as the models in (Espinoza et al., 2022; LeJeune et al., 2024; Pant et al., 2024), by, *inter alia*:

(i) Incorporating greater heterogeneity in behavior by having n behavioral compartments ($S_i, E_i, A_i, \ldots, R_i$ for $i = 1, 2, \ldots, n$). This extends the studies by Lejune et al. (LeJeune et al., 2024) (which assumes homogeneous behavior within the population), Espinoza et al. (Espinoza et al., 2022) and Pant et al. (Pant et al., 2024) (which considered a maximum of two behavioral groups for all disease compartments).
(ii) Allowing for back-and-forth transition between the n heterogeneous behavioral sub-groups (c_{ij}, where $j, i = 1, 2, \ldots, n$, and $j \neq i$). This extends the Espinoza et al. study (Espinoza et al., 2022) (where no such transitions are allowed between the two behavioral groups considered therein).
(iii) Incorporating the dynamics of hospitalized individuals (i.e., adding equations for the dynamics of the compartments H_i, for $i = 1, 2, \ldots, n$). The dynamics of hospitalized individuals are not accounted for in the models presented in (Espinoza et al., 2022; LeJeune et al., 2024; Pant et al., 2024).
(iv) Using a time-dependent transmission parameter ($c_i^A(t)$, with $i = 1, \ldots, n$) to account for group-level change of behavior in response to the level of hospitalization in the community. This extends the studies in (Espinoza et al., 2022; Pant et al., 2024) (which used fixed parameters for behavior change in response to the disease).
(v) Assuming that recovery from infection does not induce permanent immunity against future infection (i.e., $\xi \neq 0$). This extends the studies in (Espinoza et al., 2022; Pant et al., 2024) (which assume recovery from natural infection induces permanent immunity against future infection).

The basic qualitative properties of the behavior model (2.1) will now be explored below.

2.1. Basic qualitative properties of the multigroup model

Consider the following biologically feasible region for the model (2.1):

$$\Omega = \left\{ (S_1, \ldots, S_n, E_1, \ldots, E_n, \ldots, R_n) \in \mathbb{R}_+^{6n} : 0 \leq \sum_{i=1}^{n} (S_i + E_i + I_{a,i} + I_{s,i} + I_{h,i} + R_i) \leq N(0) \right\},$$

where $N(0) = \sum_{i=1}^{n} (S_i(0) + E_i(0) + I_{a,i}(0) + I_{s,i}(0) + I_{h,i}(0) + R_i(0))$ is the total initial size of the population. We claim the following result:

Theorem 2.1. *Suppose that the initial values $S_i(0)$, $E_i(0)$, $I_{a,i}(0)$, $I_{i,i}(0)$, $I_{h,i}(0)$, $R_i(0)$ for $i = 1, \ldots, n$ of the model (2.1) are non-negative, with $S_i(0) > 0$ for at least some i. Then, the solutions*

$$S_i(t), E_i(t), I_{a,i}(t), I_{i,i}(t), I_{h,i}(t), R_i(t) \text{ for } i = 1, \ldots, n$$

of the model are bounded for all time $t \geq 0$. Furthermore, the region Ω is positively invariant with respect to the flow generated by the behavior model (2.1).

Proof. To prove the boundedness of the model, it is convenient to obtain the equation for the rate of change of the total population (obtained by adding all the equations of the model), given by:

$$\frac{dN}{dt} = -\delta_h \sum_{i=1}^{n} I_{h,i}(t).$$

Since all the parameters and state variables of the model are non-negative (consequently, $\delta_h \geq 0$ and $I_{h,i}(t) \geq 0$ for all t, with $i = 1, \ldots, n$), it follows from the above equation that:

$$\frac{dN}{dt} \leq 0, \quad \text{for all } t \geq 0. \tag{2.3}$$

It follows, by solving the differential inequality (2.3) subject to the initial condition $N(0) = N_0$, that $N(t)$ is bounded above by N_0. Since $S_i(t) > 0$ for some i and all $t \geq 0$, the total population, $N(t)$, is bounded below by zero. Hence, $0 < N(t) \leq N_0$, meaning $N(t)$ is bounded. Since $N(t)$ is bounded, it follows that all the state variables of the model are bounded. Thus, all solutions of the model (2.1) are bounded in Ω for all time $t \geq 0$. Since all solutions of the model are bounded in Ω (i.e., all initial solutions in Ω remain in Ω for all time t), the region Ω is positively invariant with respect to the flow generated by the model (2.1). □

The implication of Theorem 2.1 is that the behavior model (2.1) is well-posed mathematically and epidemiologically in the bounded and positively invariant region Ω (Hethcote, 2000). Hence, it is sufficient to study its qualitative dynamics in the region Ω.

3. Special case with two behavioral groups

For practical application and illustrative purposes, a special case of the n-group behavior model with two behavioral groups (i.e., equation (2.1) with $n = 2$) will be considered and rigorously analyzed. The equations for this special case, tagged the *2-group behavior model*, are given by equation (A.1) of Appendix B.

3.1. Existence and stability of disease-free equilibria of the 2-group model

3.1.1. Existence

The 2-group behavior model (A.1) has the following disease-free equilibria, which always exist:

(i) **nontrivial disease-free equilibria (NTDFE)**

$$(S_1^*, E_1^*, I_1^*, A_1^*, H_1^*, R_1^*, S_2^*, E_2^*, I_2^*, A_2^*, H_2^*, R_2^*) = (kp, 0, 0, 0, 0, 0, (1-k)p, 0, 0, 0, 0, 0), \tag{3.1}$$

where $0 \leq k \leq 1$ and p is the total population size at equilibrium. These equilibria are classified as follows.

(a) ($k = 1$) the resulting disease-free equilibrium, termed the *Group 1-only* disease-free equilibrium, is denoted by *G1DFE*.
(b) ($k = 0$) the resulting disease-free equilibrium, called the *Group 2-only* disease-free equilibrium, is denoted by *G2DFE*.
(c) ($0 < k < 1$) the resulting disease-free equilibrium, termed the *coexistence* disease-free equilibrium, is denoted by *G3DFE*.

(ii) **trivial disease-free equilibrium (TDFE)**

$$(S_1^*, E_1^*, I_1^*, A_1^*, H_1^*, R_1^*, S_2^*, E_2^*, I_2^*, A_2^*, H_2^*, R_2^*) = (0, 0, 0, 0, 0, 0, 0, 0, 0, 0, 0, 0). \tag{3.2}$$

Since this *extinction* equilibrium is not epidemiologically realistic (i.e., no humans at steady-state), it will not be analyzed for its stability.

The stability of the three nontrivial disease-free equilibria of the 2-group model will now be analyzed.

3.1.2. Stability of the nontrivial disease-free equilibria of the 2-group model

The stability of the three nontrivial DFE of the 2-group behavior model (G1DFE, G2DFE, and G3DFE) will be analyzed using standard linearization. Owing to the large size of the 2-group behavior model (making the computation of the eigenvalues of its Jacobian evaluated at the respective DFE less tractable mathematically), the linearization approach will be combined with

some results related to the properties of Metzler matrices (Berman et al., 1989; Farina & Rinaldi, 2000). In particular, the notations in (Kamgang & Sallet, 2008) will be used. It is convenient to recall the following definitions (from (Kamgang & Sallet, 2008)).

Definition 3.1. A matrix $M \in \mathbb{R}^{n\times n}$ is called a Metzler matrix if all of its off-diagonal entries are nonnegative.

Definition 3.2. A matrix $M \in \mathbb{R}^{n\times n}$ is called Hurwitz stable if the real part of all eigenvalues of M are strictly negative.

Definition 3.3. A matrix $M \in \mathbb{R}^{n\times n}$ is called Metzler stable if it is a Metzler matrix with Hurwitz stability (i.e., the real part of all eigenvalues of M are strictly negative).

Define the following quantity:

$$\mathbb{R}_c = \theta_l\left(\frac{r\beta_i}{\sigma_i} + \frac{(1-r)\beta_a}{\gamma_a} + \frac{rq\beta_h}{\gamma_h + \delta_h}\right). \tag{3.3}$$

Lastly, it is convenient to define the additional parameter

$$\Gamma = c_{12}^B \Big/ c_{21}^B,$$

which will be called the *relative influence ratio* of behavioral Group 1 to behavioral Group 2. We claim the following result:

Theorem 3.4. *The Group 1–only disease-free equilibrium of the 2-group behavior model* (A.1) *is stable whenever* $\mathbb{R}_c < 1$ *and* $\Gamma > 1$. *The G1DFE is unstable whenever* $\mathbb{R}_c > 1$ *or* $\Gamma \leq 1$.

The proof of Theorem 3.4 is given in Appendix B. Similarly, the following results can be established for the stability of the G2DFE and the G3DFE (the proofs are not given here to save space).

Theorem 3.5. *The Group 2–only disease-free equilibrium of the 2-group behavior model* (A.1) *is stable whenever* $\mathbb{R}_c < 1$ *and* $\Gamma < 1$, *and unstable whenever* $R_c > 1$ *or* $\Gamma \geq 1$.

Theorem 3.6. *The coexistence disease-free equilibrium of the 2-group behavior model* (A.1) *is stable whenever* $\mathbb{R}_c < 1$ *and* $\Gamma = 1$, *and is unstable whenever* $R_c > 1$ *or* $\Gamma \neq 1$.

The epidemiological implication of Theorems 3.4–3.6 is that a small influx of COVID-19-infected individuals will not generate a large outbreak of COVID-19 in the community if $\mathbb{R}_c$ is less than unity. The quantity $\mathbb{R}_c$ is the *control reproduction number* of the 2-group model (A.1), which represents the average number of new COVID-19 infections generated by an infectious individual introduced into a population where non-pharmaceutical public health interventions (such as lockdown measures) are implemented (Anderson & May 1992; Hethcote, 2000). In the absence of non-pharmaceutical interventions (i.e., $\theta_l = 1$), the control reproduction number $\mathbb{R}_c$ reduces to

$$\mathbb{R}_0 = \mathbb{R}_c|_{\theta_l=1} = \frac{r\beta_i}{\sigma_i} + \frac{(1-r)\beta_a}{\gamma_a} + \frac{rq\beta_h}{\gamma_h + \delta_h}, \tag{3.4}$$

where $\mathbb{R}_0$ is the *basic reproduction number* of the model (A.1) (which measures the average number of new infections generated by an infectious individual introduced into a completely susceptible population). The results of Theorems 3.4–3.6 are numerically illustrated in Fig. 3, where numerous initial conditions of the model are shown to converge to one of the three nontrivial disease-free equilibria when $\mathbb{R}_c < 1$.

When $\mathbb{R}_c > 1$, simulations suggest that all initial solutions of the 2-group model (A.1) converge to the TDFE (see Fig. 4). Hence, the 2-group behavior model (A.1) undergoes a transcritical bifurcation at $\mathbb{R}_c = 1$. This result is a consequence of the fact that the 2-group behavior model (A.1) is an epidemic model, which assumes a closed population (no immigration or emigration), no demographics (no birth rate or natural death rate) and recovery from COVID-19 infection does not induce permanent immunity against future infections (i.e., $\xi \neq 0$). Under these assumptions, every member of the community will acquire infection and succumb to the disease, and (since there is no replenishment or influx of new susceptible individuals into the community, by birth or immigration) the population will eventually die out. This does not happen when $\xi = 0$, meaning when infection *does* induce permanent immunity, the disease dies out while the population does not (see Figure C.1 in Appendix C).

The results of Theorems 3.4–3.6, along with the simulations in Fig. 4, are numerically illustrated in Fig. 5, showing the stability regions of the disease-free equilibria (G1DFE, G2DFE, G3DFE, TDFE) for various values of the control reproduction number, $\mathbb{R}_c$, and the relative influence ratio, Γ.

3.2. Data fitting and parameter estimation for the 2-group model (A.1)

The 2-group behavior model (A.1) has 15 original parameters (the lockdown parameter θ_l will be redefined as four separate parameters, based on lockdown phases in New York City as described below). The baseline values of ten of these original parameters are known from the literature. The 2-group behavior model will now be fitted to the observed daily

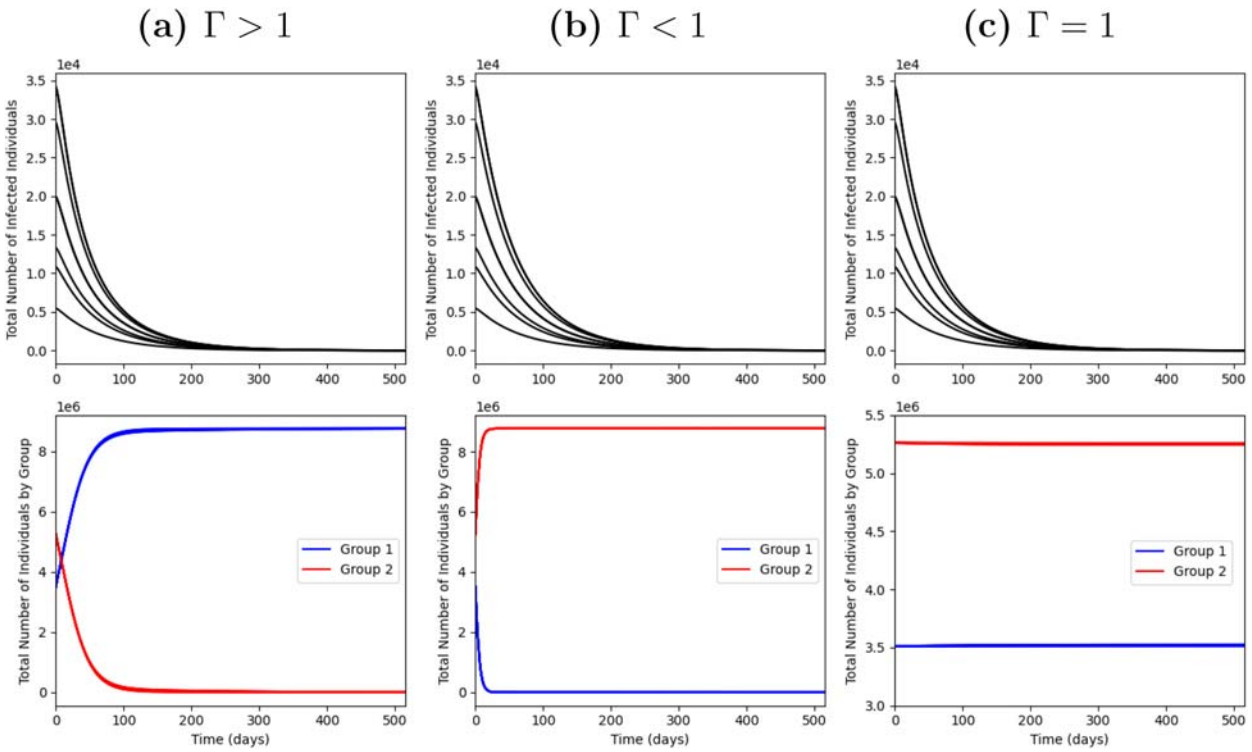

Fig. 3. Simulations of the 2-group behavior model (A.1), showing the profile of the total number of infected individuals (top) and the total number of individuals in the community, stratified by behavioral group ($N_1(t)$ and $N_2(t)$)(bottom), as a function of time for various initial conditions. Column (a): $c_{12}^B = 0.5, c_{21}^B = 0.25$ ($\Gamma = 2 > 1$). Column (b): $c_{12}^B = 0.25, c_{21}^B = 0.5$ ($\Gamma = 0.5 < 1$). Column (c): $c_{12}^B = c_{21}^B = 0.5$ ($\Gamma = 1$). In all panels, all other parameter values used in these simulations are as given in Tables 3 and 4, but with $\theta_l = 1$, $\beta_a = 0.1$, and $\beta_i = 0.05$ (so that, $\mathbb{R}_c = 0.78 < 1$). These simulations show that when $\mathbb{R}_c < 1$, solutions of model (A.1) converge to G1DFE if $\Gamma > 1$ (see Figure(a)), G2DFE if $\Gamma < 1$ (see Figure(b)), and G3DFE if $\Gamma = 1$ (see Figure(c)), in line with Theorems 3.4–3.6.

hospitalization data (which was smoothed into 7-day running average data) for New York City (NYC Health, 2023) during the first wave of the COVID-19 pandemic to estimate the five unknown parameters. For notational convenience, the known parameters of the 2-group behavior model are categorized as *fixed* parameters, and the unknown parameters of the 2-group behavior model are categorized as *fitted* parameters. Furthermore, for model fitting purposes, the following five time intervals or phases for the implementation of the COVID-19 lockdown measures in New York City are considered (Ferré-Sadurní, 2020; Amid ongoing COVID, 2020; Amid ongoing COVID-19 pandemic, 2020; Feuer & Newman, 2020; Governor Cuomo announces New York, 2020; Gold and Ferré-Sadurní; Jacobs; Cuomo, 2020):

(a) Phase 0 (*pre-lockdown phase*): time period from January 20, 2020 (day of the index case in the US) to the beginning of initial lockdown (March 13, 2020, (Ferré-Sadurní, 2020)). For this phase, the lockdown parameter, θ_l, is set to 1 (i.e., no lockdown measures were implemented in New York City).
(b) Phase 1 (*initial lockdown phase*): this accounts for the time period from March 14, 2020 to April 4, 2020, (Amid ongoing COVID, 2020; Amid ongoing COVID-19 pandemic, 2020) when initial lockdown measures were implemented in New York City. Here, the lockdown parameter is represented by $\theta_{l,1}$, which will be fitted.
(c) Phase 2 (*hard lockdown phase*): this accounts for the time period from April 5, 2020 to May 27, 2020 (Feuer & Newman, 2020; Governor Cuomo announces New York, 2020), when stringent lockdown measures were implemented in New York City. Here, the lockdown parameter is represented by $\theta_{l,2}$, which will be fitted.
(d) Phase 3 (*first re-opening phase*): this accounts for the time period from May 28, 2020 to August 25, 2020 (Gold and Ferré-Sadurní; Jacobs; Cuomo, 2020), when some of the lockdown measures were lifted in New York City. Here, the lockdown parameter is represented by $\theta_{l,3}$, which will be fitted.
(e) Phase 4 (*second/final re-opening phase*): this accounts for the time period from August 25, 2020 onward when more lockdown measures were lifted. Here, the lockdown parameter is represented by $\theta_{l,4}$, whose value will be obtained from fitting the model with data.

Thus, based on these lockdown implementation phases, the NPI parameter, θ_l, in the model (A.1) is now explicitly defined in terms of the following piecewise-defined function:

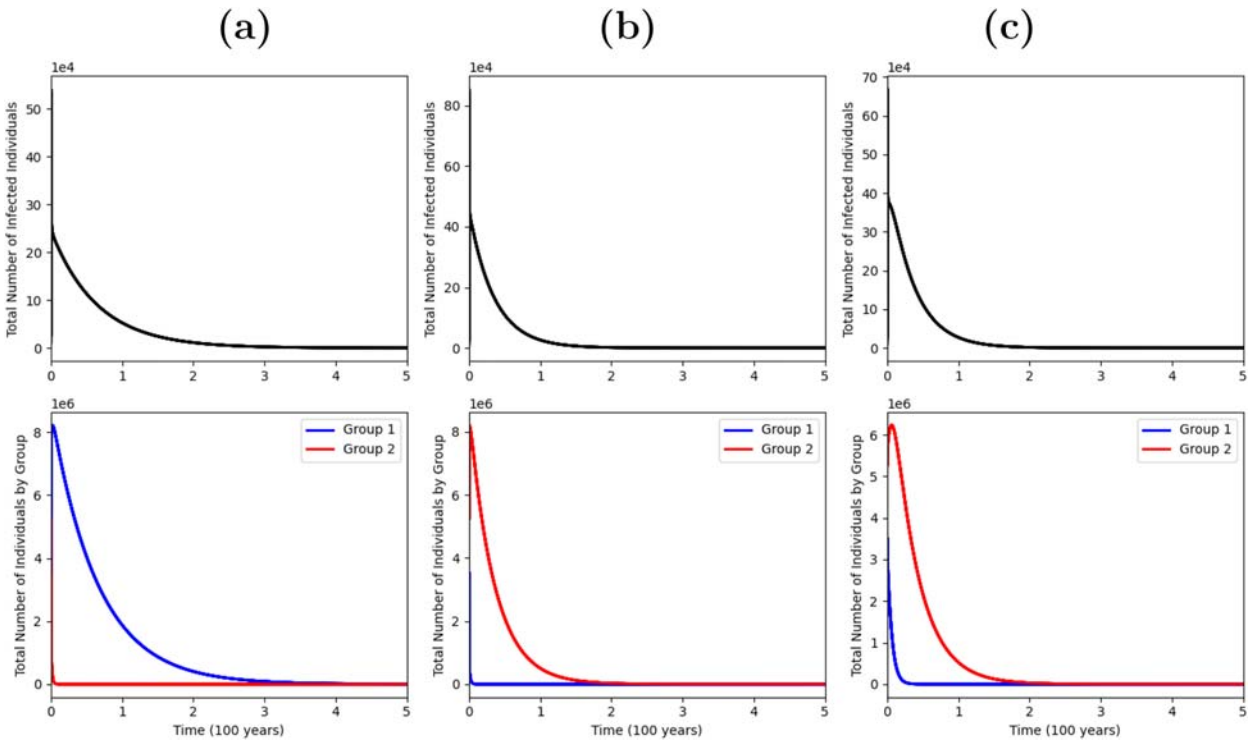

Fig. 4. Simulations of the 2-group behavior model (A.1), showing the profile of the total number of infected individuals (top) and the total number of individuals in the community, stratified by behavioral group ($N_1(t)$ and $N_2(t)$)(bottom), as a function of time for various initial conditions. Column (a): $c_{12}^B = 0.5, c_{21}^B = 0.25$ ($\Gamma = 2 > 1$). Column (b): $c_{12}^B = 0.25, c_{21}^B = 0.5$ ($\Gamma = 0.5 < 1$). Column (c): $c_{12}^B = c_{21}^B = 0.5$ ($\Gamma = 1$). All other parameter values used in these simulations are as given in Tables 3 and 4, but with $\theta_l = 1$, $\beta_a = 1$, and $\beta_i = 0.5$ (so that, $\mathbb{R}_c = 7.8 > 1$). These simulations show that when $\mathbb{R}_c > 1$, solutions of the 2-group model (A.1) converge to the extinction equilibrium (TDFE), regardless of the value of Γ.

$$\theta_l = \begin{cases} 1 & \text{during Phase 0} \\ \theta_{l,1} & \text{during Phase 1} \\ \theta_{l,2} & \text{during Phase 2} \\ \theta_{l,3} & \text{during Phase 3} \\ \theta_{l,4} & \text{during Phase 4} \end{cases} \tag{3.5}$$

This will result in three additional ($\theta_{l,i}$ for $i = 2, 3, 4$) unknown parameters to be fitted, causing the 2-group behavior model (A.1) to have a total of 18 parameters. The values of the fixed parameters of the 2-group behavior model (A.1) used in fitting it to the observed data (NYC Health, 2023) are briefly described below.

3.2.1. Baseline values of the fixed parameters of the 2-group model (A.1)

The baseline values of all the disease-related parameters of the 2-group behavior model (A.1) have been estimated in the literature. For instance, the effective contact rate for disease transmission by asymptomatically infectious individuals (β_a) during the first wave of the COVID-19 pandemic in the United States is estimated to be between 0.34 and 0.72 per day (Gumel, Iboi, Ngonghala, & Ngwa, 2021; Ngonghala et al., 2021). Similarly, the transmission rate for symptomatic infectious individuals (β_i) during the same period is estimated to be between 0.36 and 0.45 per day (Ngonghala et al., 2021; Pant & Gumel, 2024). The rate of transition out of the exposed class (σ_e) to the asymptomatic-infectious class or symptomatically infectious class has been estimated to be 1/4 per day (Lauer et al., 2020; Li et al., 2020). The proportion (r) of these exposed individuals who show clinical symptoms of the disease at the end of the exposed period is estimated to be 0.6 (Brozak et al., 2021). The rate of transition out of the symptomatic-infectious class (σ_i) is estimated to be 1/14 per day (Tang et al., 2020), and the proportion, q, of symptomatic infectious individuals who are hospitalized is estimated to be 0.05 (Griffin et al., 2024). Dan et al. (Dan & Mateus, 2021) estimated the rate of loss of infection-acquired immunity (ξ) during the first wave of the COVID-19 pandemic to be 1/180 per day. Furthermore, asymptomatic and hospitalized individuals recover within 9 and 10 days, respectively (so that, $\gamma_a = 1/9$ per day and $\gamma_h = 1/10$ per day) (Kissler et al., 2020; Tang et al., 2020). Finally, individuals hospitalized with COVID-19 during the first wave of the pandemic suffer disease-induced mortality (δ_h) at a rate 0.41 per day (Macedo et al., 2021). The baseline values of these fixed parameters of the 2-group model (A.1) are tabulated in Table 3.

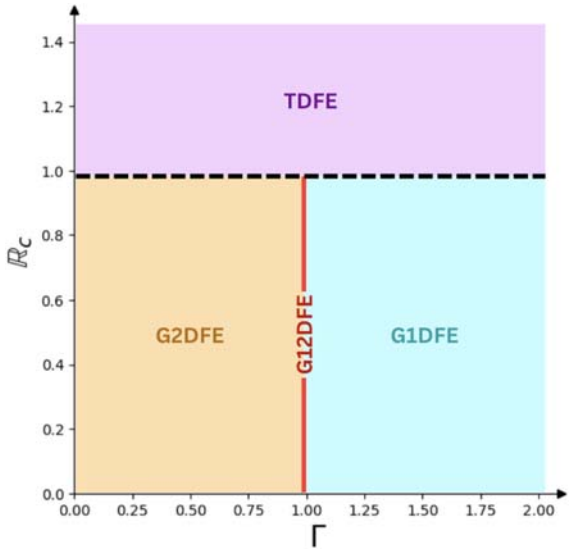

Fig. 5. Stability regions of different disease-free equilibria of the 2-group behavior model (A.1), as determined by the values of the control reproduction number $\mathbb{R}_c$ and the relative influence ratio Γ. This figure shows that the 2-group behavior model (A.1) has a bifurcation at $\mathbb{R}_c = 1$ and a separatrix at $\Gamma = 1$.

Table 3
Baseline values of the fixed parameters of the 2-group model (A.1) during the first wave of the COVID-19 pandemic in New York City.

Parameter	Baseline value	Source
β_a	0.625 day^{-1}	(Gumel, Iboi, Ngonghala, & Ngwa, 2021; Ngonghala et al., 2021)
β_s	0.375 day^{-1}	(Ngonghala et al., 2021; Pant & Gumel, 2024)
ξ	1/180 day^{-1}	Dan & Mateus, (2021)
σ_e	1/4 day^{-1}	(Lauer et al., 2020; Li et al., 2020)
σ_s	1/14 day^{-1}	Tang et al. (2020)
γ_a	1/9 day^{-1}	Tang et al. (2020)
γ_h	1/10 day^{-1}	Kissler et al. (2020)
r	0.6 (dimensionless)	Brozak et al. (2021)
q	0.05 (dimensionless)	Griffin et al. (2024)
δ_h	0.41 day^{-1}	Macedo et al. (2021)

3.2.2. Values of estimated parameters of the 2-group model obtained from data fitting

The 2-group behavior model (A.1) is fitted to the 7-day moving average of the observed daily COVID-19 hospitalization data for the City of New York during the first wave of the pandemic (NYC Health, 2023) by using a suitable optimization method to estimate the eight unknown parameters (namely, the four behavior-related parameters: a_1, a_2, c_{12}^B, c_{21}^B, and the four phased lockdown implementation parameters: $\theta_{l,1}$, $\theta_{l,2}$, $\theta_{l,3}$, and $\theta_{l,4}$, defined in equation (3.5)). In particular, the BFGS algorithm with sum of squared errors as the loss function (embedded in the LMFit library in python, and chosen due to its fast convergence rate and robustness in handling noisy data and local minima (Dai, 2002)) is used due to fit the 2-group behavior model (A.1)). The results obtained from fitting the model to the 7-day running average hospitalization data (NYC Health, 2023) are depicted in Fig. 6. This figure shows a very good fit of the 2-group model (blue curve) to the observed 7-day moving average of the daily hospitalization data for New York City (red dots) for the fitting period (i.e., the time period between February 29th, 2020 and July 28th, 2020). The estimated values of the *fitted parameters* (obtained from fitting the 2-group behavior model (A.1) with the data), together with their associated 95 % confidence intervals, are tabulated in Table 4. The accuracy of the fitted 2-group model is assessed by using it to predict the second wave of the COVID-19 pandemic in New York City. To do this, the 2-group behavior model (A.1) is simulated using the fixed and estimated parameters in Tables 3 and 4, respectively, and compared with the available (withheld for cross validation purposes) 7-day running average hospitalization data for the second wave. The results obtained, depicted to the right of the dashed vertical black line of this figure, showed that the fitted model (green curve) almost perfectly predicts the second wave (red dots to the right of the dashed vertical black line). This fits the data with an R^2 value of 0.9691 (with adjusted $R^2 = 0.9674$), confirming the goodness of the fit (Ezekiel, 1930).

It can be seen from Table 4 that individuals in Group 1 reduce their contacts ($c_1^A(t)$), defined in (2.2)) at a rate much faster than that of individuals in Group 2 ($c_2^A(t)$), defined in (2.2)). This is because the estimated value of the exponent, a_1 (for the hospitalization-induced behavioral change for the individuals in Group 1), tabulated in Tables 4 and is much higher (almost 3 times) than that of the exponent, a_2 (for the hospitalization-induced behavioral change for Group 2). It should be noted that

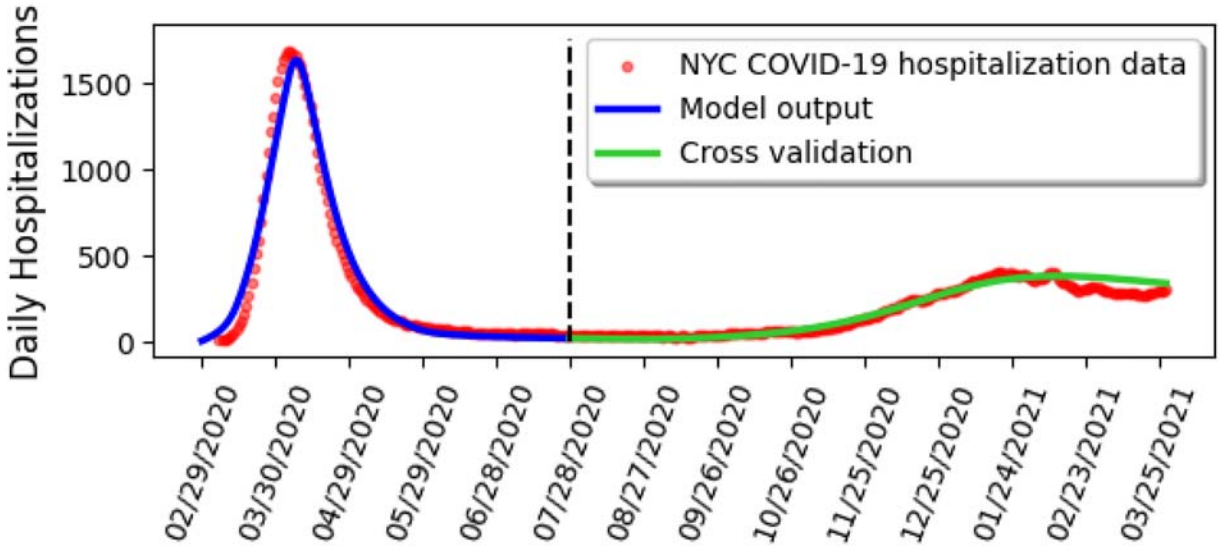

Fig. 6. Data fitting and cross validation of the 2-group behavior model (A.1), using the 7-day running average daily hospitalization data for New York City (NYC Health, 2023) (red dots), carried out using the BFGS algorithm. The values of the fixed parameters of the 2-group model, used in fitting it with the data, are given in Table 3, and the values of the estimated parameters of the 2-group model (obtained from the data fitting), together with their associated 95 % confidence intervals, are given in Table 4. The data fitting (blue curve) is carried out using the data from the first 150 days after the index case in New York City (i.e., from February 29, 2020 to July 28, 2020), while the cross-validation (green curve) is carried out using the following eight months worth of data (i.e., from July 29, 2020 to March 25, 2021). The eight unknown parameters of the 2-group model were estimated from the data fitting to the model, and their estimated values are tabulated in Table 4.

individuals in Group 2 also reduce their risk-taking behavior in response to the level of hospitalization in the community (albeit only slightly). The profile of estimated contact rates for individuals in Group 1 ($c_1^A(t)$; solid blue curve) and Group 2 ($c_2^A(t)$; dashed blue curve) is shown in Fig. 7, along with simulated daily hospitalizations ($I_h(t)$) in the population (computed using the 2-group behavior model (A.1) with parameters in Tables 3 and 4, shown in red). This figure shows that, at the peak of the COVID-19 hospitalizations in New York City during the first wave (highlighted by the yellow shaded region), individuals in Group 1 dramatically decreased their daily contacts (by about 80 %, compared to their baseline contact rate; see the solid blue curve at the peak of the red curve). In contrast, individuals in Group 2 only decreased their daily contacts by about 40 % during the same period (see the dashed blue curve, at the peak of the red curve). A similar phenomenon occurred at the peak of the second wave (highlighted by the shaded purple region), but with the individuals in Group 1 decreasing contacts only by about to 30 % (in comparison to their baseline), while Group 2 individuals only decreased their contacts by a little more than 10 % (in comparison to the baseline). The lower reduction in contacts during the second wave of the COVID-19 pandemic in New York City may have been a result of masking fatigue (Newman, 2020), or perhaps the relatively lower hospitalization rate during this time period (as compared to the first wave) resulted in a lower perception of risk.

Table 4 also shows that the rate at which individuals in Group 2 change their behavior and become *more cautious* (c_{12}^B) is much higher (3-fold) than the rate at which cautious individuals (i.e., those in Group 1) change their behavior and become less cautious (c_{21}^B). Although the estimated value of the influence parameter c_{12}^B is larger than that of the parameter c_{21}^B, the relative influence of Group 1 (given by $c_{12}^B \frac{N_1(t)}{N(t)}$) is initially small (due to the small initial size of Group 1; note that, in the formulation of the model (A.1), it was assumed that the majority of the population is in Group 2 during the early stages of the epidemic) when compared to the relative influence of Group 2 (given by $c_{21}^B \frac{N_2(t)}{N(t)}$) throughout the first wave. However, as Group 1 begins to increase in size (particularly during the summer of 2020), the relative sizes of the behavioral groups begin to change rapidly (see the shaded yellow and purple regions of Fig. 8), with Group 1 ultimately overtaking Group 2 around February of 2021 (with 70 % of the population ending up in Group 1 by March 2021, while the rest of the population (30 %) remained in Group 2). In other words, Fig. 8 shows that, despite its initial small size, Group 1 ultimately became dominant (i.e., the vast majority of individuals in the community significantly reduced their risk-taking behavior and adhered to public health interventions) by the second wave of the pandemic. Finally, Table 4 also shows that the efficacy of the lockdown measures implemented in New York City during Phase 1 was low (with efficacy, $1 - \theta_{l,1}$, estimated to be around 0.25; that is, 25 %), but increased dramatically to nearly 100 % during the second phase (i.e., $1 - \theta_{l,2} \approx 1$). The efficacy decreased during subsequent phases (down to 85 % and 70 % during Phases 3 and 4, respectively). Thus, Table 4 confirms that non-pharmaceutical interventions (NPIs) and mitigation measures were not effectively implemented in New York City during the first phase (due, perhaps, in large part, to the lack of clarity and consistency in messaging, and pandemic preparedness (Lander, 2021)). However, NPIs were effectively implemented by Phase 2, although this was not generally maintained during Phases 3 and 4 (potentially due to increasing levels of interventions fatigue and spread of misinformation and disinformation about the pandemic (Newman, 2020)).

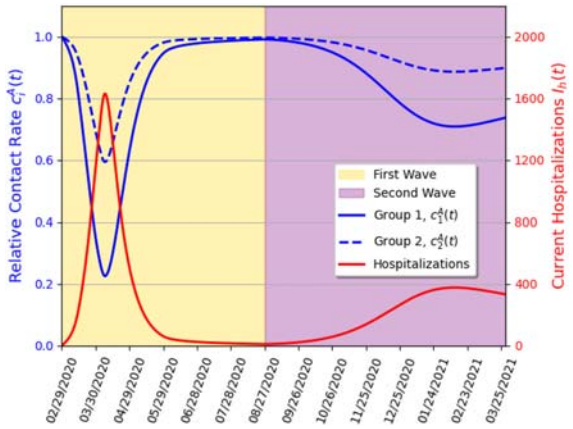

Fig. 7. Profile of the relative contact rates ($c_i^A(t)$ for $i = 1, 2$) as compared with the number of hospitalized individuals over time ($I_h(t)$). This figure is generated by solving the 2-group behavior model (A.1), using the fixed and estimated parameters given in Tables 3 and 4, respectively (to obtain the value of $I_h(t)$ for each t), together with the estimated values of the parameters a_1 and a_2 (given in Table 4) to compute the relative contact rate multipliers for individuals in Group 1 ($c_1^A(t)$, solid blue curve) and Group 2 ($c_2^A(t)$, dashed blue curve) over time. The number of individuals who are currently hospitalized ($I_h(t)$) is depicted by the red curve. The time periods of the first and second waves are represented by the shaded yellow and purple regions, respectively.

Table 4
Baseline values of the estimated parameters for the 2-group behavior model (A.1), obtained by fitting it to the 7-day running average data of daily hospitalizations in New York City (NYC Health, 2023) from February 29, 2020 to July 28, 2020 using the BFGS algorithm. The values of the fixed parameters of the 2-group model, used in the fitting of the model, are given in Table 3. The asterisk (*) represents a fixed value given for the upper bound of the behavioral parameter a_1. The python software used to generate the confidence intervals was unable to determine an upper bound for this parameter. As a result, the fixed upper bound of $a_1 = 800,000$ was chosen (this is 100 times the baseline value of a_1; there is only a marginal change in the value of the quantity $c_1^A(t)$, defined in (2.2), for all values of a_1 greater than the chosen value of 800, 000).

Parameter	Baseline value	95 % CI
a_1	8000 (dimensionless)	(7923.4,800000*)
a_2	2800 (dimensionless)	(2790.7,7923.4)
c_{12}^B	1/30 day^{-1}	(0.031,0.036)
c_{21}^B	1/90 day^{-1}	(0.0087,0.014)
$\theta_{l,1}$	0.74664 (dimensionless)	(0.65,0.75)
$\theta_{l,2}$	0.00133 (dimensionless)	(0,0.0061)
$\theta_{l,3}$	0.15427 (dimensionless)	(0.15,0.16)
$\theta_{l,4}$	0.30970 (dimensionless)	(0.29,0.34)

The estimated values of the four behavior-related parameters (a_1, a_2, c_{12}^B, and c_{21}^B) were obtained by fitting the 2-group behavior model (A.1) to the 7-day moving hospitalization average data (NYC Health, 2023). Ideally, these parameters should be estimated by fitting this model with behavior data, which was not widely collated and made publicly available until several months into the pandemic. As a result, 7-day running average hospitalization data were used to estimate the four behavioral parameters of the 2-group behavior model (A.1). However, as behavioral data (in the form of mask compliance on the subway in New York City (MTA subway and bus mask, 2024)) became available starting in June 2020, the accuracy of the data fitting is further corroborated by comparing the results obtained (by simulating the model (A.1) with parameters given in Tables 3 and 4) for the relative contact rates with this behavioral data. The results obtained (depicted in Fig. 9) validate the fitted values of a_1 and a_2 by showing qualitatively similar curves between population contact rates ($c_1^A(t)$ for Group 1, $c_2^A(t)$ for Group 2, and the weighted average contact rate $N(t)(\frac{c_1^A(t)}{N_1(t)} + \frac{c_2^A(t)}{N_2(t)})$ for the full population) and the percentage of noncompliant (with respect to masking) individuals in the population. The trends observed in each of these curves suggest that as attitudes towards the disease shift and individuals decrease their relative contacts (and become more cautious in general), the noncompliant portion of the population decreases.

Values of $\mathbb{R}_c$ for the 2-group behavior model (A.1) during the four lockdown phases: The baseline values of the fixed and fitted parameters in Tables 3 and 4 are now used to compute the values of the control reproduction number ($\mathbb{R}_c$, given by equation (3.3)) for New York City during Phases 1 through 4 of lockdown, and the results obtained are tabulated in Table 5. This table shows a more pronounced outbreak during Phase 1 (measured in terms of higher values of $\mathbb{R}_c$; for this phase, $\mathbb{R}_c \approx 4$). This value of $\mathbb{R}_c$, which is in line with estimates from other modeling studies for the COVID-19 outbreak in New York City during the first wave (Sy et al., 2021; Yue et al., 2021), is to be expected for a community where the efficacy of the lockdown and other NPIs implemented is low (e.g., $1 - \theta_{l,1} = 0.25$, as estimated for New York City during this period, in Table 4). This resulted in a devastating first wave for New York City, which ran during the period between March 2020 and the end of July of 2020 (i.e., Phases 1 and 2), causing 52, 899 hospitalizations and 23, 590 deaths (NYC Health, 2023). Although the value of $\mathbb{R}_c$ decreased dramatically (due to the stringent implementation of these control measures during Phase 2), it quickly rebounded during Phases 3 and 4 when the control measures were progressively relaxed (in particular, relaxation of

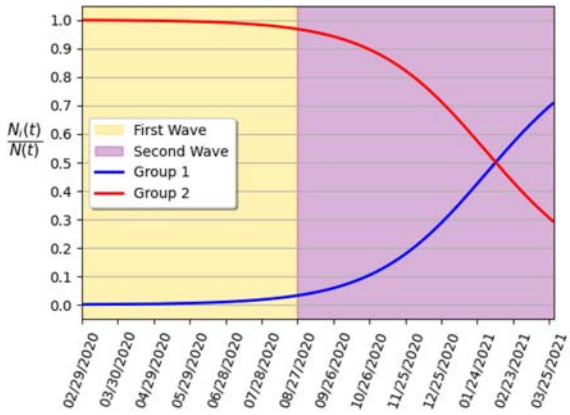

Fig. 8. Profile of the relative group sizes ($N_i(t)/N(t)$ for $i = 1, 2$) over time. This figure is generated by solving the 2-group behavior model (A.1), using the fixed and estimated parameters given in Tables 3 and 4, respectively (to obtain the values of $N_1(t)$ and $N_2(t)$ for each t) to compute the population dynamics for Group 1 ($\frac{N_1(t)}{N(t)}$, blue curve) and Group 2 ($\frac{N_2(t)}{N(t)}$, red curve) over time. The time periods of the first and second waves are represented by the shaded yellow and purple regions, respectively.

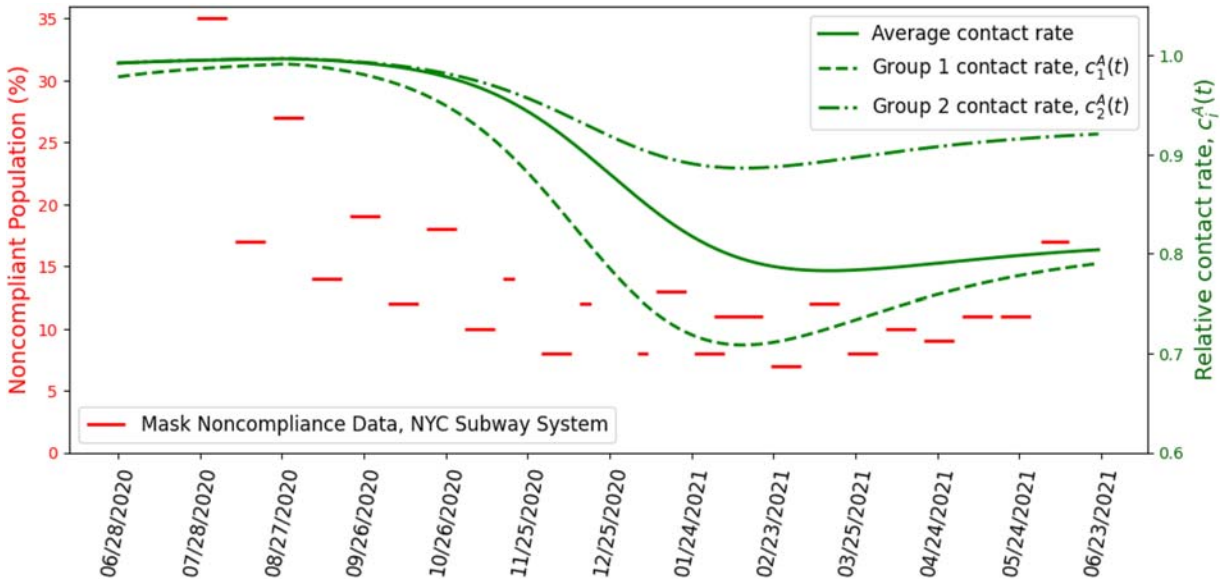

Fig. 9. Profile of the contact rates ($c_1^A(t)$ and for $c_2^A(t)$) of individuals in the two behavioral groups, as a function of time, during the first two waves of the COVID-19 pandemic, superimposed on data for mask noncompliance on the New York City subway system (MTA subway and bus mask, 2024). Parameter values used in the simulations are as given in Tables 3 and 4 The purple curve represents the relative contact rate of individuals in the risk-taking group (Group 2, $c_2^A(t)$); the gold curve represents the relative contact rate of individuals in the cautious group (Group 1, $c_1^A(t)$); and the green curve represents the population average relative contact rate ($\frac{N_1(t)}{N(t)}c_1^A(t) + \frac{N_2(t)}{N(t)}c_2^A(t)$). The profiles are compared with empirical data for mask non-compliance in New York City during the same period (shown in red dashed lines, with each dash corresponding to the data collection period).

lockdown measures during Phase 4 resulted in the second wave, albeit the second wave was much milder than the first wave observed in New York City during Phases 1 and 2). Finally, in order to quantify the importance of explicitly incorporating heterogeneous human behavior in accurately capturing the trajectory of the COVID-19 pandemic and making realistic predictions, a *behavior-free* equivalent of the 2-group behavior model (A.1), obtained by setting all the behavior-related parameters of the model to zero, is now explored (by fitting the resulting behavior-free model with the same 7-day moving average of the daily hospitalization data for New York City during the first wave (NYC Health, 2023), as discussed below). The objective is to compare which of the two models (behavior or behavior-free) best captures the observed dynamics (or burden) of the pandemic in New York City during the first wave, and predicts the trajectory and burden of the pandemic during the second wave.

Table 5
Values of the control reproduction number $\mathbb{R}_c$ for the 2-group behavior model (A.1) (see equation (3.3)) during the four lockdown phases of the pandemic in New York City for model (A.1). Parameter values used in computing these values are as given in Tables 3 and 4

Phase	Duration	$\mathbb{R}_c$
Phase 1	March 14, 2020 to April 4, 2020	4.045
Phase 2	April 5, 2020 to May 27, 2020	0.016
Phase 3	May 28, 2020 to August 25, 2020	0.929
Phase 4	After August 25, 2020	1.539

3.3. Data fitting and parameter estimation for the behavior-free model (A.2)

Setting the four behavior-related parameters (a_1, a_2, c_{12}^B, and c_{21}^B) of the 2-group behavior model (A.1) to zero gives the 1-group *behavior-free* (homogeneous) model, given by the system of nonlinear differential equations in equation (A.2) of Appendix A. As a result, only the four lockdown parameters ($\theta_{l,i}$ for $i = 1, \ldots, 4$, where $1 - \theta_{l,i}$ measures the efficacy of Phase i lockdowns and NPIs) will be fitted. It should be noted that, unlike in the case of the 2-group behavior model (A.2), the 1-group (homogeneous) behavior-free model (A.2) has no reduction in contacts due to the level of COVID-19 hospitalizations in the community. Fig. 10 depicts the results of fitting the behavior-free model (A.2) with the 7-day running average of daily hospitalization data (the values of the estimated parameters obtained from fitting this model to the data are tabulated in Table 6). Fig. 10 shows that, although the behavior-free model (A.2) fits the data for the first wave of the pandemic in New York City reasonably well, it fails to accurately capture the dynamics of the second wave. Furthermore, unlike the 2-group behavior model (A.1), which accurately captures the disease dynamics during both waves (see Fig. 6), the behavior-free model (A.2) over-estimated the recorded 7-day running average of daily hospitalizations during the period from winter 2020 to spring 2021 (see the green curve in Fig. 10). Specifically, the behavior-free model over-estimated the reported daily 7-day running average of hospitalizations at the end of the second wave (on March 25, 2021) by 104 %. On the other hand, the 2-group behavior model (A.1) was within 10 % of the recorded 7-day running average of hospitalizations for this date. Hence, it can be concluded that epidemiological models that do not explicitly incorporate the effect of human behavior changes may fail to accurately capture the trajectory (as well as predict the future course) of the COVID-19 pandemic in a community, such as New York City during the first two waves of the pandemic. The computed AIC (Akaike Information Criteria) (Akaike, 1974) values for the behavior model (A.1) and the behavior-free model (A.2) are 3182.9 and 3844.8, respectively, confirming the superiority of the former over the latter in capturing and predicting the disease dynamics in New York City during the two waves. This is in line with some recent modeling studies that highlight the importance of incorporating human behavior into models for the spread of respiratory pathogens (Espinoza et al., 2022; LeJeune et al., 2024; Pant et al., 2024).

It is also worth noting from Table 6 that the estimated value of the NPI implementation parameter during Phase 1 ($\theta_{l,1}$), generated from fitting the behavior-free model (A.2), is much lower ($\theta_{l,1} = 0.45$) than the corresponding value obtained from fitting the 2-group behavior model (A.1) (where $\theta_{l,1} = 0.74$). In other words, in order for the behavior-free model (A.2) to fit the

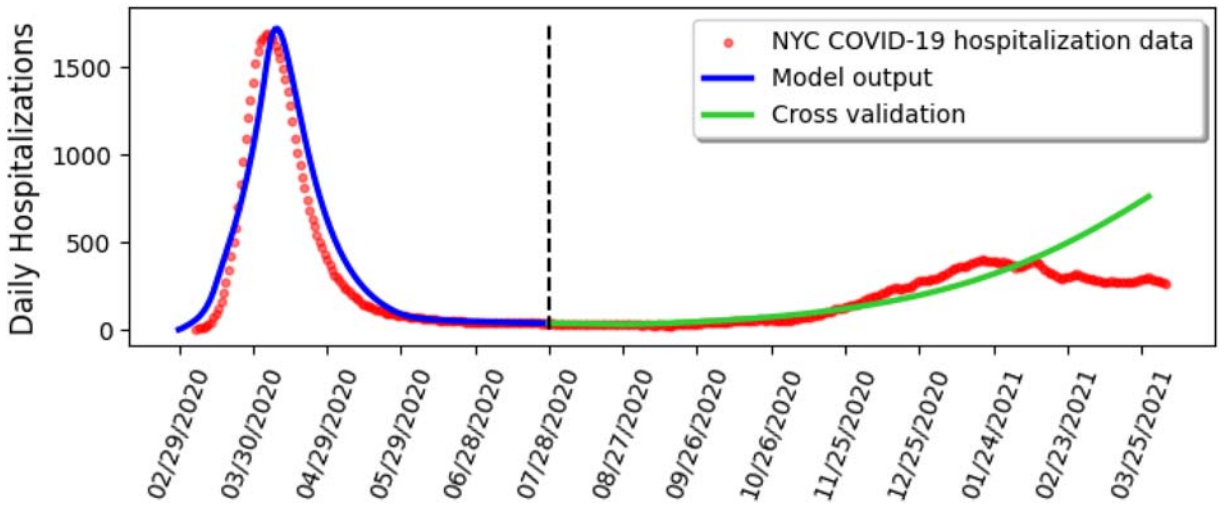

Fig. 10. Data fitting and cross validation of the behavior-free model (A.2), using the 7-day running average daily hospitalization data for New York City (red dots) (NYC Health, 2023), carried out using the BFGS algorithm. The values of the fixed parameters of the behavior-free model, used in fitting it to the data, are given in Table 3, and the values of the estimated parameters of the model (obtained from the fitting) are given in Table 6. The fitting (blue curve) is carried out using the data for the first 150 days after the index case in New York City (i.e., from February 29, 2020 to July 28, 2020), while the cross-validation (green curve) is carried out using the subsequent eight months worth of data (i.e., from July 29, 2020 to March 25, 2021). The four unknown parameters of the behavior-free model ($\theta_{l,1}$, $\theta_{l,2}$, $\theta_{l,3}$, $\theta_{l,4}$) were estimated from fitting the model with the data, and their estimated values are tabulated in Table 6.

Table 6
Baseline values of the estimated parameters of the behavior-free model (A.2) (with fixed parameters as given in Table 3) obtained by fitting the model to the 7-day running average data of daily hospitalizations in New York City (NYC Health, 2023) for the period from February 29, 2020 to July 28, 2020 using the BFGS algorithm.

Parameter	Baseline value
$\theta_{l,1}$	0.45 (dimensionless)
$\theta_{l,2}$	0.0153 (dimensionless)
$\theta_{l,3}$	0.178 (dimensionless)
$\theta_{l,4}$	0.248 (dimensionless)

first wave data accurately, the estimated efficacy of NPIs in curtailing the pandemic in New York City during the first phase had to be quite high (about 55 %). This is significantly higher than the estimated efficacy of this parameter obtained from fitting the behavior model with the first wave data (which was about 26 %). It is reasonable to conclude that the behavior-free model may have over-estimated the efficacy of the NPI implementation during the early stages of the first wave of the COVID-19 pandemic in New York City (since media reports suggest considerable inconsistency and lack of clarity in messaging in New York City during this period (Lander, 2021)). Thus, in addition to over-estimating the hospitalization burden during the second wave, the behavior-free model may have over-estimated the effectiveness of NPI measures implemented in New York City during the first phase of the COVID-19 pandemic. However, the estimated values of the NPI parameters during Phases 2 through 4 ($\theta_{l,2}$, $\theta_{l,3}$, $\theta_{l,4}$), obtained from fitting the behavior and behavior-free models, were similar (see Tables 4 and 6). In other words, both the 2-group behavior model and the 1-group behavior-free model gave similar (and possibly reasonable) estimates for the effectiveness of NPIs during subsequent phases of the COVID-19 pandemic (from April 4, 2020 to March 25, 2021) in New York City.

Values of $\mathbb{R}_c$ for the behavior-free model (A.2) during the four lockdown phases: Here the fixed and fitted parameters for the behavior-free model (A.2), tabulated in Tables 3 and 6, are used to compute the values of the control reproduction number ($\mathbb{R}_c$) associated with the behavior-free model, given by equation (3.3). The results obtained are given in Table 7. It should be noted that the aforementioned low estimate of the NPI parameter (i.e., high efficacy of NPIs) during Phase 1 of the pandemic reduces the value of the control reproduction number ($\mathbb{R}_c$) to 2.43, as against the value $\mathbb{R}_c = 4.045$ estimated from fitting the 2-group behavior model (compare Tables 5 and 7).Since the 2-group behavior model (A.1) has been shown to be more realistic in capturing the correct trajectory and burden of the pandemic (in comparison to the more parsimonious behavior-free equivalent (A.2)), the remainder of this study will focus on the 2-group behavior model (A.1). To determine what parameters have the greatest impact on the 2-group behavior model (A.1) (measured in terms of some chosen public health outcome metrics, such as peak daily hospitalizations and cumulative mortality), detailed global sensitivity analysis of the 2-group behavior model, with respect to the chosen health outcome metrics, will now be carried out.

3.4. Sensitivity analysis for the 2-group behavior model (A.1)

Having calibrated and validated the 2-group behavior model (A.1), the next step is to conduct a global sensitivity analysis to determine which of its 18 parameters have the highest impact on a chosen response function. Since the reproduction

Table 7
Values of the control reproduction number $\mathbb{R}_c$ for the behavior-free model (A.2) during the four lockdown phases of the COVID-19 pandemic in New York City. Parameter values used to compute the values of $\mathbb{R}_c$ are as given in Tables 3 and 6

Phase	Duration	$\mathbb{R}_c$
Phase 1	March 14, 2020 to April 4, 2020	2.43
Phase 2	April 5, 2020 to May 27, 2020	0.083
Phase 3	May 28, 2020 to August 25, 2020	0.961
Phase 4	After August 25, 2020	1.339

Table 8
COVID-19 related peak daily hospitalizations and cumulative mortality in New York City at the end of the first wave of the pandemic and after the second wave of the pandemic, generated by simulating the 2-group behavior model (A.1) using the values of the fixed and estimated parameters given in Tables 3 and 4, respectively. Initial conditions used in the simulations are given by $S_1(0) \approx kN(0)$ and $S_2(0) \approx (1-k)N(0)$ for various values of $k \in [0, 1]$.

Proportion	First Wave		Second Wave	
initially in Group 1 (k)	Peak Daily Hospitalizations	Cumulative Mortality	Peak Daily Hospitalizations	Cumulative Mortality
0	1630	17,914	376	25,993
0.2	1253	13,959	250	15,720
0.4	1034	11,750	250	15,180
0.6	898	10,465	251	14,670
0.8	804	9565	251	14,265
1	736	8756	251	14,135

thresholds of the 2-group behavior model (denoted by $\mathbb{R}_c$ and $\mathbb{R}_0$, given by equations (3.3) and (3.1.2), respectively) do not include the behavior-related parameters of the model, a sensitivity analysis will be carried out with respect to two distinct disease burden-related metrics: (a) peak daily COVID-19 hospitalizations and (b) cumulative mortality, during the first and second waves of the pandemic in New York City. In particular, the sensitivity analysis will be conducted using partial rank correlation coefficients (PRCCs), which entails defining each of the 18 parameters of the 2-group behavior model (A.1) as a distribution (typically uniform) over a range (or an interval). Following (Gao et al., 2023), each parameter range is determined by taking 40 % to the left and to the right of its baseline value (tabulated in Tables 3 and 4). To ensure broad and efficient exploration of the parameter space, a Latin Hypercube Sampling (LHS) approach is used (Blower & Dowlatabadi, 1994; Marino et al., 2008; McLeod et al., 2006; Smith et al., 2005). This method entails stratifying the range of each of the 18 parameters of the chosen response function into 1000 equally spaced intervals and selecting parameter values such that each interval is sampled only once per parameter. This results in an 18-dimensional hypercube, from which a set of 1000 parameter vectors is drawn. PRCC values range from -1 to 1, with positive PRCC values indicating positive correlation with the chosen response function, and negative PRCC values indicating negative correlation. A higher magnitude PRCC value (say, a value greater than 0.5 or less than -0.5) signifies a stronger correlation (McLeod et al., 2006).

The results for the sensitivity analysis, obtained using the baseline values and ranges of the parameters of the 2-group behavior model given in Table 9, are tabulated, for two snapshots of time during the first two waves of the pandemic in New York City (namely, towards the end of the first wave, April 20, 2020; and towards the end of the second wave, February 21, 2021), in Figs. 11 and 12, respectively (the exact PRCC values are given in Table 10 in Appendix C).

3.4.1. Sensitivity analysis with respect to the peak daily hospitalization

Fig. 11(a) shows that the top five parameters of the 2-group behavior model (A.1) that have the most influence on peak daily hospitalizations during the first wave of the COVID-19 pandemic in New York City (April 20, 2020) are:

(i) The maximum effective contact rate for asymptomatic infectious individuals (β_a; PRCC $= +0.849$).
(ii) The maximum effective contact rate for symptomatic infectious individuals (β_i; PRCC $= +0.842$).
(iii) The effectiveness of government-mandated community lockdowns (and other NPIs) during Phase 1 of the pandemic in New York City ($\theta_{l,1}$; PRCC $= +0.806$).
(iv) The rate of progression of individuals leaving the exposed class (σ_e; PRCC $= +0.786$).
(v) The proportion of symptomatic individuals that are hospitalized (q; PRCC $= +0.576$).

Thus, peak daily hospitalizations in New York City during the first wave of the pandemic can be significantly reduced by implementing intervention and mitigation strategies that decrease maximum effective contact rates (β_a and β_i) and the proportion of symptomatic individuals that are hospitalized (q), and increasing the efficacy of Phase 1 government-mandated community lockdowns and NPIs ($1 - \theta_{l,1}$). The effective contact rate parameters (β_a and β_i) can be decreased by, for instance, reducing contacts, large scale random testing, quarantine/isolation, and the use of face masks in public. Similarly, $\theta_{l,1}$ can be increased by increasing the coverage and effectiveness of the NPIs implemented. Finally, the parameter q can be decreased by early detection and effective treatment of symptomatic individuals. The transition parameter σ_e is primarily biological, which

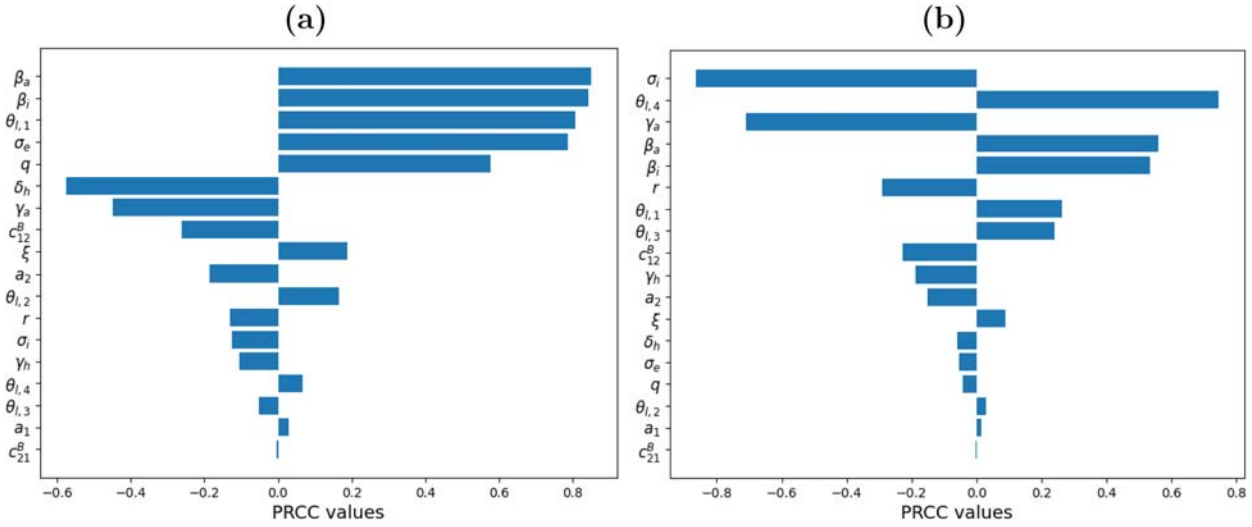

Fig. 11. Partial Rank Correlation Coefficient (PRCC) values for the 18 parameters of the model (A.1) with respect to peak daily hospitalizations at (a) April 2020 and (b) February 2021 using parameter intervals as given in Table 9. Exact PRCC values are given in Table 10(a) in the Appendix.

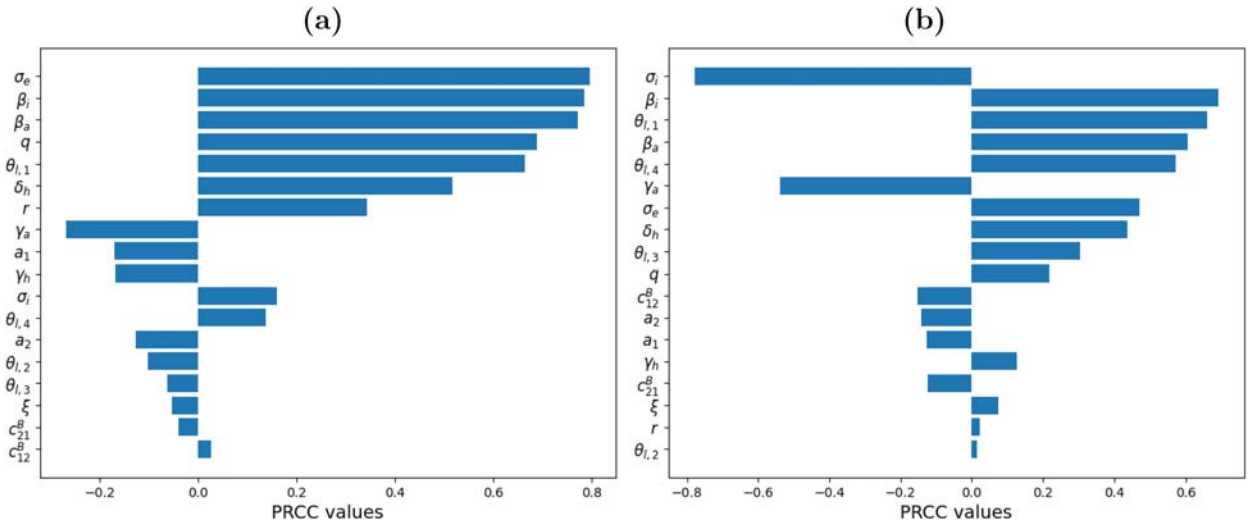

Fig. 12. Partial Rank Correlation Coefficient (PRCC) values for the 18 parameters of the model (A.1) with respect to cumulative mortality at (a) April 2020 and (b) February 2021 using parameter intervals as given in Table 9. Exact PRCC values are given in Table 10(b) in the Appendix.

may depend on the immune status of the infected host. To the authors' knowledge, there is no specific intervention at the moment that can specifically target this parameter, except, perhaps, if a future pharmaceutical intervention (e.g., a therapeutic drug) that can delay newly-infected individuals from developing clinical symptoms of the disease or becoming infectious is developed.

Fig. 11(b) shows that the top five parameters that have the most influence on this response metric during the second wave (February 21, 2021) are:

(i) The rate of progression of individuals leaving the symptomatic infectious class (σ_i; PRCC $= -0.864$).
(ii) The parameter for the measure of effectiveness of the government-mandated community lockdowns (and other NPIs) during Phase 4 of the pandemic in New York City ($\theta_{l,4}$; PRCC $= +0.744$).
(iii) The rate at which asymptomatically infectious individuals recover (γ_a; PRCC $= -0.711$).
(iv) The maximum effective contact rate for asymptomatic infectious individuals (β_a; PRCC $= +0.561$).
(v) The maximum effective contact rate for symptomatic infectious individuals (β_i; PRCC $= +0.535$).

Thus, two of the top five parameters that affect peak daily hospitalizations during the first wave (β_a and β_i) also remain relevant during the second wave, while the parameters $\theta_{l,1}$ (for the measure of effectiveness of the government-mandated community lockdowns in Phase 1), σ_e (for the rate at which individuals leave the exposed class), and q (for the proportion of symptomatic individuals that are hospitalized) diminish in relevance with respect to peak daily hospitalizations during the second wave. Unlike the first wave, three additional parameters (σ_i, the rate of progression of individuals leaving the symptomatic infectious class; $\theta_{l,4}$, the measure of effectiveness of the government-mandated community lockdowns in Phase 4; and γ_a, the rate at which asymptomatically infectious individuals recover) become relevant during the second wave (where their PRCC values increased in comparison to their values during the first wave by about 7-fold, 11- fold, and 1.6-fold, respectively). In other words, this study shows that, during the second wave of the COVID-19 pandemic in New York City, the peak daily hospitalizations are significantly decreased with increasing values of σ_i (the rate at which symptomatically infectious individuals leave the symptomatic class), $1 - \theta_{l,4}$ (the efficacy of Phase 4 government-mandated community lockdowns and NPIs) and γ_a (the rate at which asymptomatically infectious individuals recover). Thus, peak daily hospitalizations in New York City during the second wave of the pandemic can be significantly reduced using the approaches discussed above, as well as by implementing intervention and mitigation strategies that minimize the amount of time the average individual spends in the symptomatic class ($1/\sigma_i$). This could be achieved by effective treatment of symptomatic individuals.

3.4.2. Sensitivity analysis with respect to cumulative mortality

It can be seen from Fig. 12(a) that the top five parameters of the behavior model (A.1) that have the most influence on cumulative mortality during the first wave of the COVID-19 pandemic in New York City (April 20, 2020) are:

(i) The rate of progression of individuals leaving the exposed class (σ_e; PRCC $= +0.796$).

(ii) The maximum effective contact rate for symptomatic infectious individuals (β_i; PRCC = +0.785).
(iii) The maximum effective contact rate for asymptomatic infectious individuals (β_a; PRCC = +0.772).
(iv) The proportion of symptomatic individuals that are hospitalized (q; PRCC = +0.690).
(v) The parameter for the measure of effectiveness of government-mandated community lockdowns (and other NPIs) during Phase 1 of the pandemic in New York City ($\theta_{l,1}$; PRCC = +0.665).

As these are the same parameters as listed in Section 3.4.1, for influence on peak daily hospitalizations at the end of the first wave of the COVID-19 pandemic in New York City, similar approaches as listed there would lead to a decrease in first wave mortality.

Fig. 12(b) shows that the top five parameters that have the most influence on this response metric during the second wave (February 21, 2021) are:

(i) The rate of progression of individuals leaving the symptomatic infectious class (σ_i; PRCC = −0.778).
(ii) The maximum effective contact rate for symptomatic infectious individuals (β_i; PRCC = +0.691).
(iii) The parameter for the measure of effectiveness of government-mandated community lockdowns (and other NPIs) during Phase 1 of the pandemic in New York City ($\theta_{l,1}$; PRCC = +0.661).
(iv) The maximum effective contact rate for asymptomatic infectious individuals (β_a; PRCC = +0.606).
(v) The parameter for the measure of effectiveness of government-mandated community lockdowns (and other NPIs) during Phase 4 of the pandemic in New York City ($\theta_{l,4}$; PRCC = +0.572).

Thus, cumulative mortality in New York City during the second wave of the COVID-19 pandemic can be significantly reduced using the strategies mentioned in Section 3.4.1, as well as by implementing strategies to increase the efficacy of Phase 4 government-mandated community lockdown (and other non-pharmaceutical intervention measures), given by $(1 - \theta_{l,4})$. This could be achieved through a slower re-opening process, in tandem with public health campaigning to combat mask fatigue.

3.5. Numerical simulations of the 2-group behavior model (A.1)

In this section, the population-level impact of the four behavioral parameters (a_1, a_2, c_{12}^B and c_{21}^B) on the trajectory and burden of the COVID-19 pandemic in New York City during the first two waves will be assessed. Such simulations provide a scientific basis for determining which of the factors that induce behavioral change (namely, disease-motivated, as measured by a_1 and a_2; and peer influence-motivated, as measured by c_{12}^B and c_{21}^B) is more influential in affecting the trajectory and burden of the disease during the two waves. Determining the behavioral change factors that have the most influence on disease trajectory and burden will be critical in shaping public health policy and messaging, as identified factors may be targeted for public health intervention (for instance, if the hospitalization-induced behavioral change factor is determined to be more influential than the peer influence-induced behavioral change factor, then public health messaging resources should be prioritized for making hospitalization-related information widely available to the public). The objective of this section is achieved by simulating the 2-group behavior model (A.1) with the fixed and estimated parameters in Tables 3 and 4, respectively, for various values of the four behavioral change parameters as described below.

3.5.1. Impact of hospitalization-induced behavior change parameters (a_1 and a_2)

The simulation results obtained from running the 2-group behavior model (A.1) with various values of the hospitalization-induced behavior change parameters a_1 and a_2 (using the parameters in Tables 3 and 4), depicted in Fig. 13, show that the number of peak daily hospitalizations during the first wave of the COVID-19 pandemic in New York City dramatically decreases with increasing values of a_2 (see Fig. 13(a)). This figure also shows that changes in a_1 have little to no effect on the peak daily hospitalizations during the first wave. The dominance of the contact rate modifier for Group 2 (a_2) over that of Group 1 (a_1) on decreasing the peak daily hospitalizations during the first wave is likely due to the fact that the size of Group 2 was larger than that of Group 1 during the first wave. For example, Fig. 13(a) shows that a 25 % reduction in the peak daily hospitalizations during the first wave can be attained if the baseline value of a_2 is increased by 15 %. A similar result was obtained for the peak daily hospitalizations during the second wave (Fig. 13(b)). This figure shows that, despite the decrease in the relative size of Group 2 between the first two waves of the pandemic in New York City (see Fig. 8), the contact rate modifier for Group 2 (a_2) still had a significant effect on the peak daily hospitalizations during the second wave. This result is in line with the sensitivity analysis conducted in Section 3.4.1, where the PRCC value of a_2 with respect to the peak daily hospitalizations increased (in magnitude) from −0.185 in April 2020 (i.e., during the first wave) to −0.443 in February 2021 (i.e., during the second wave). However, Fig. 13(b) also shows that behavior change by individuals in Group 1 had a more pronounced impact on reducing the peak daily hospitalizations during the second wave, in comparison to its impact during the first wave (compare Fig. 13(a) and (b)).

Simulations for the effect of the hospitalization-induced behavior change parameters (a_1 and a_2) on the cumulative COVID-19 mortality during the first wave (depicted in Fig. 13(c)) show a similar pattern to their effect on the peak daily

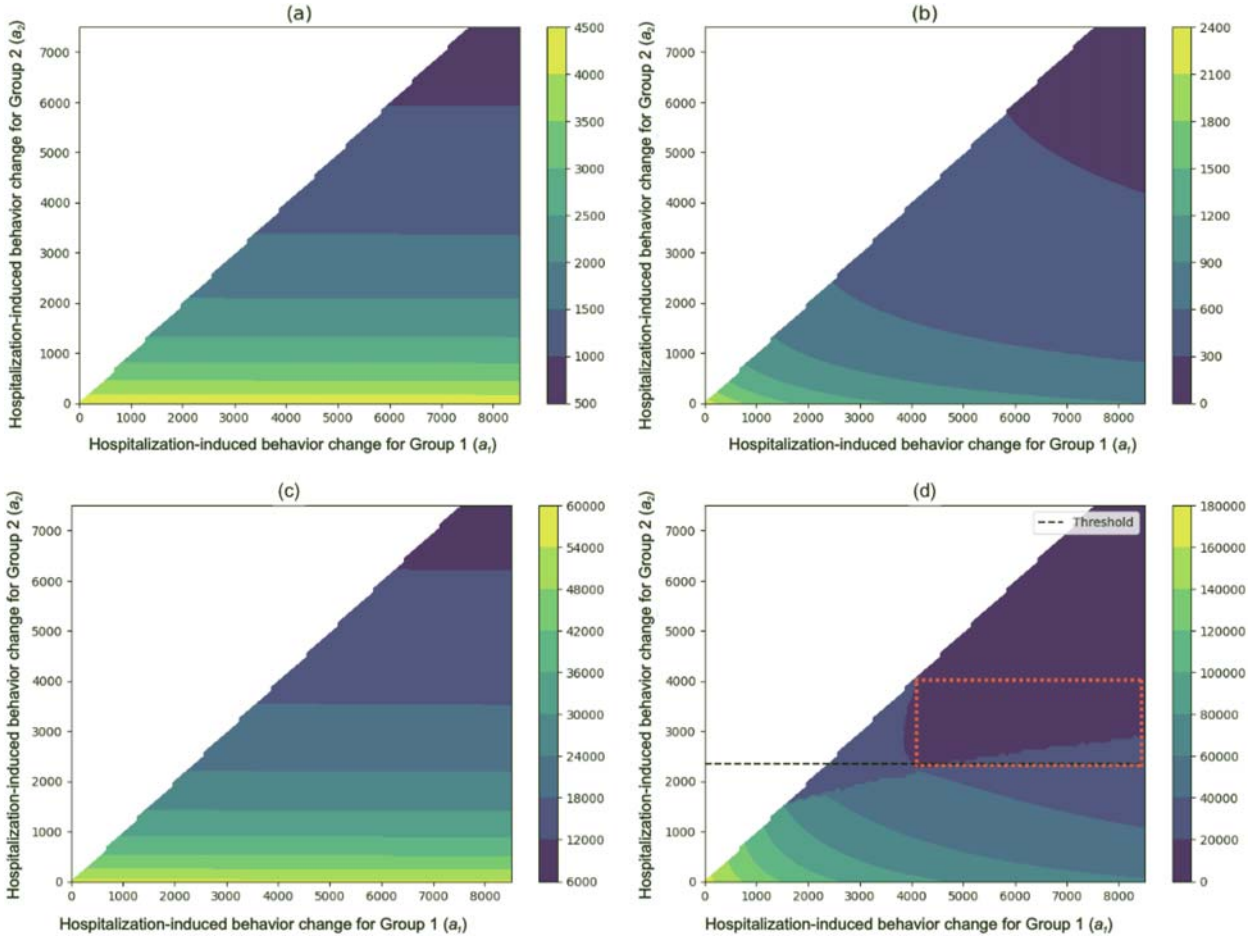

Fig. 13. Effect of the hospitalizations-induced behavior change parameters, a_1 and a_2, on the peak daily hospitalizations and cumulative mortality in New York City during the first two waves of the COVID-19 pandemic. Simulations of the behavior model (A.1) with the baseline parameter values in Tables 3 and 4, and various values of a_1 and a_2. (a) Effect of a_1 and a_2 on the peak daily hospitalizations during the first wave. (b) Effect of a_1 and a_2 on the peak daily hospitalizations during the second wave. (c) Effect of a_1 and a_2 on the cumulative mortality during the first wave. (d) Effect of a_1 and a_2 on the cumulative mortality during the second wave. The black line labeled "threshold" indicates a value of a_2 above which a significant reduction in the cumulative mortality can be achieved. The dotted red box highlights a region in the a_1-a_2 plane within which an increase in a_1 leads to an increase in the cumulative COVID-19 mortality.

hospitalizations during the first wave (depicted in Fig. 13(a)). For the cumulative mortality metric, Fig. 13(c) further shows that achieving a 25 % reduction in cumulative COVID-19 mortality during the first wave would require at least a 25 % increase (from baseline value of 2800 to 3500) in the value of the contact rate modifier for Group 2, a_2 (as against the 15 % increase in the baseline value of the same parameter to achieve the 25 % reduction in peak daily hospitalizations for the scenario depicted in Fig. 13(a)). These simulations show that, during the first wave of the pandemic, a more pronounced positive behavior change in Group 2 (i.e., increase in the value of a_2) was needed to significantly minimize the cumulative COVID-19 mortality in New York City during this wave. However, during the second wave, a significantly lower threshold value of a_2 exists ($a_2 \approx 2,200$), above which the aforementioned significant reduction in the cumulative mortality can be achieved (Fig. 13(d)). Furthermore, there exists a region in the a_1-a_2 plane ($4,100 \leq a_1 \leq 8,000, 2,200 \leq a_2 \leq 4,000$; see red box in Fig. 13(d)) within which an increase in a_1 leads to an increase in the cumulative COVID-19 mortality. This may be due to the fact that, in this region in the a_1-a_2 plane (unlike in all other regions in Fig. 13(d)), an increase in a_1 prolongs the duration of the second wave (see Figure C.2 in Appendix C).

3.5.2. *Impact of peer influence-induced behavioral change parameters (c_{12}^B and c_{21}^B)*

The simulation results obtained from running the 2-group behavior model (A.1) with various values of the influence-related behavior change parameters, c_{12}^B and c_{21}^B (using the parameters in Tables 3 and 4), are depicted in Fig. 14. In particular, Fig. 14(a) shows that the number of peak daily hospitalizations during the first wave of the COVID-19 pandemic in New York City was far more affected by the behavior of Group 2 (measured in terms of the average time it takes an individual in Group 2 to change their behavior and move to Group 1, as a result of interaction with individuals in Group 1, given by $1/c_{12}^B$)

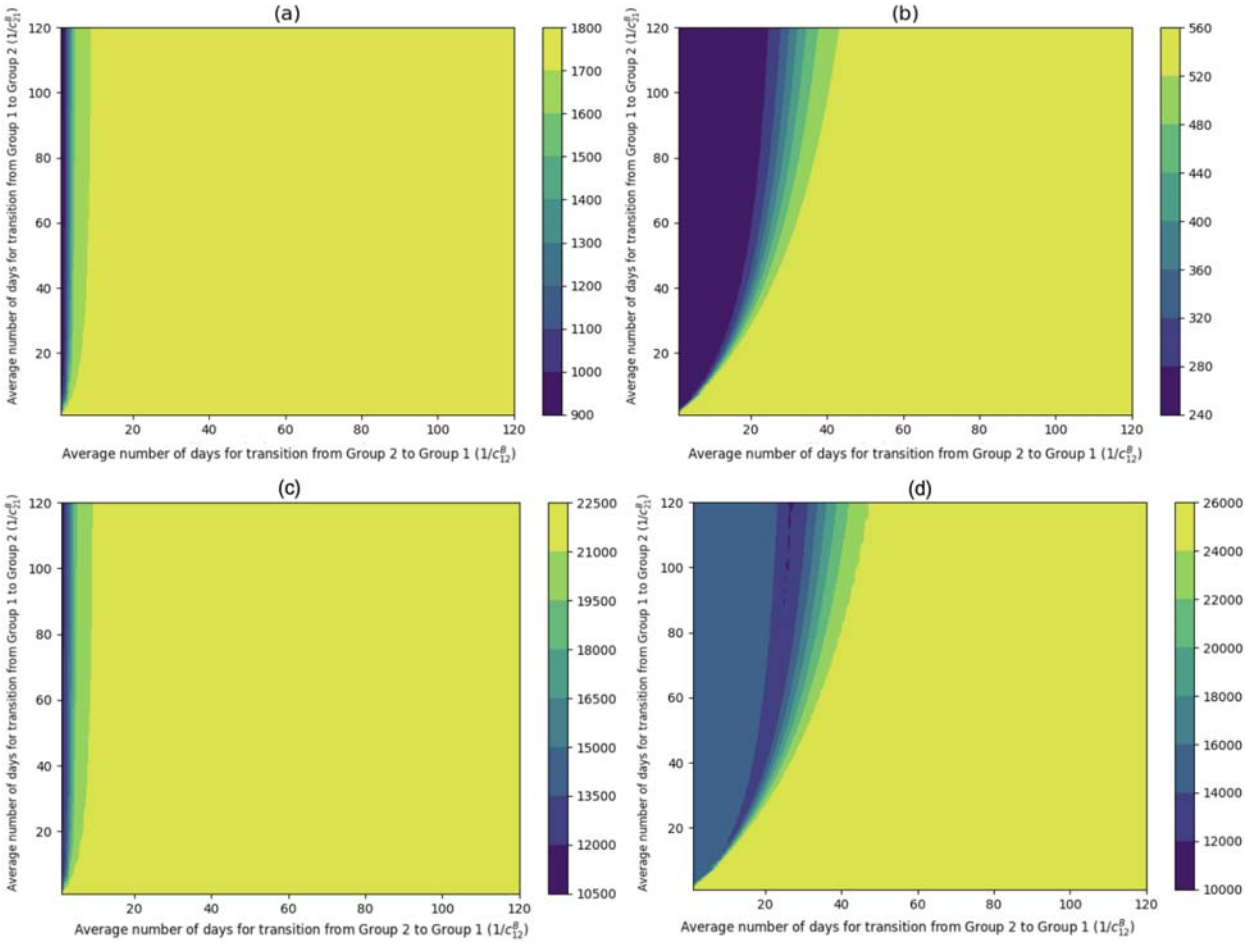

Fig. 14. Effect of the peer influence-induced behavior change parameters, c_{12}^B and c_{21}^B, on the peak daily hospitalizations and cumulative mortality in New York City during the first two waves of the COVID-19 pandemic. Simulations of the 2-group behavior model (A.1) with the baseline parameter values in Tables 3 and 4, and various values of c_{12}^B and c_{21}^B. (a) Effect of c_{12}^B and c_{21}^B on the peak daily hospitalizations during the first wave. (b) Effect of c_{12}^B and c_{21}^B on the peak daily hospitalizations during the second wave. (c) Effect of c_{12}^B and c_{21}^B on the cumulative mortality during the first wave. (d) Effect of c_{12}^B and c_{21}^B on the cumulative mortality during the second wave.

than it was by the behavior of Group 1. This is in line with what was observed in the corresponding simulations for hospitalization-induced behavioral changes (as shown in Fig. 13(a)). Furthermore, this figure shows that, if the average duration for individuals in Group 2 to move to Group 1 is longer than 5 days (i.e., $1/c_{12}^B > 5$), then the value of peak daily hospitalizations is essentially fixed at 1800 hospitalized individuals at the height of the first wave of the pandemic. It is worth noting from Fig. 14(a) that, even in the case where the change of behavior from Group 2 to Group 1 is almost instantaneous ($1/c_{12}^B \leq 1$ day), peak daily hospitalizations cannot be reduced above 50 % of the aforementioned baseline value of 1800. Thus, by comparing Fig. 13(a) and 14(a), it is clear that a greater reduction in the number of peak daily hospitalizations could be achieved by increases in the values of the hospitalization-induced behavioral change parameters (a_1, a_2) than by increases in the values of the influence-motivated behavioral change parameters (c_{12}^B and c_{21}^B). In other words, control strategies that focus on increasing positive behavior change with respect to hospitalization-motivated behavioral changes would have been more effective (in reducing the peak daily hospitalizations) than strategies aimed at increasing positive change with respect to influence-motivated behavioral changes during the first wave of the pandemic in New York City. During the second wave of the pandemic, the simulation results show that greater reduction in the peak daily hospitalizations (compared to during the first wave) could be achieved even if it took, on average, up to 20 days for individuals in Group 2 to change their behavior and move to Group 1 (see Fig. 14(b)). In other words, peer influence had far more effect on the peak daily hospitalizations during the second wave than during the first wave (compare Fig. 14(a) and (b)).

The simulations further show that influence rates c_{12}^B and c_{21}^B had only marginal effect on the cumulative mortality during the first wave of the pandemic in New York City, with only the most optimistic scenario ($1/c_{12}^B \approx 0$) resulting in a maximum of 50 % reduction in the cumulative mortality (see Fig. 14(c)). While this reduction is sizable, it is unrealistic to assume that most individuals would be capable of changing their attitude (and positively altering their health behaviors) so quickly. Similarly, as

seen in the case of the peak daily hospitalizations metric, the size of the COVID-19 cumulative mortality in New York City was more affected by changes in the peer influence parameters, c_{12}^B and c_{21}^B, during the second wave (compare Fig. 14(c) and (d)). Lastly, similar to what was observed in Section 3.5.1, Fig. 14(d) reveals a region in the c_{12}^B-c_{21}^B plane wherein an increase in c_{12}^B leads to an increase in cumulative mortality. This, once again, is likely due to an increase in the length of the second wave under these circumstances.

3.5.3. Impact of relative behavioral group size at the onset of the pandemic

The calibration and simulations of the 2-group behavior model (A.1) (carried out in Sections 3.2–3.5.2) were for the case where all individuals in the community started out in the risk-tolerant Group 2 before the onset of the pandemic. In this section, the model (A.1) will be simulated for scenarios where this assumption is relaxed. This relaxation of the assumption allows for the assessment of the (potentially more realistic) situation where certain members of the community are predisposed to be cautious during the very beginning of public health emergencies (this seems to have been the case in New York City during the COVID-19 pandemic (McNeil, 2020)). Specifically, the case where a proportion, $k \in [0, 1]$, of susceptible members of the community start out in Group 1 (i.e., $S_1(0) \approx kN(0)$, where $N(0)$ is the total initial population size) and the remaining susceptible proportion start out in Group 2 (i.e., $S_2(0) \approx (1-k)N(0)$) is now simulated for various values of $0 \leq k \leq 1$ (with the same parameter values in Tables 3 and 4). The simulation results show a marked decrease in daily hospitalizations ($I_h(t)$) with increasing proportion of members of the community (k) who started out in Group 1 (this reduction is particularly pronounced during the respective daily hospitalization peaks of the first and second waves). For example, a 23 % reduction of peak daily hospitalizations in the first wave can be achieved if 20 % of the susceptible members of the community started out in Group 1, in relation to the baseline scenario where every susceptible member of the community started out in Group 2 (compare red and orange curves in Fig. 15(a), and see also Table 8). Up to 55 % reduction in the peak daily hospitalizations in the first wave can be achieved if everyone started out in Group 1 (see blue curve in Fig. 15 and Table 8). Although an increase in k reduces the peak daily hospitalizations in the second wave (with an increase in k from 0 to 0.2 leading to a 33 % reduction in the peak daily hospitalizations), this reduction diminishes for $k \geq 0.2$, with $k = 0.2$ and $k = 1$ producing nearly identical values for the peak daily hospitalizations during the second wave (see purple shaded region in Fig. 15(a)). This is likely the result of similar population makeups, meaning that as long as enough individuals started out cautious at the beginning of the first wave (i.e., $k \geq 0.2$), then by the start of the second wave, the population would be mostly made up of cautious individuals ($\frac{N_1(t)}{N(t)} \approx 1$ for $t > 180$; see Figure C.4 in Appendix C). Similar results were obtained with respect to the cumulative COVID-19 mortality metric, as depicted in Fig. 15(b). This suggests that initial attitudes towards the pandemic (specifically, in the few days after the disease arrives in the community) and the government agencies responsible for public health messaging and NPI implementation have a large impact on long-term disease dynamics. Hence the early implementation of effective public health messaging that encourages a sizable proportion of the susceptible population to adhere to NPIs will significantly reduce the burden of the pandemic.

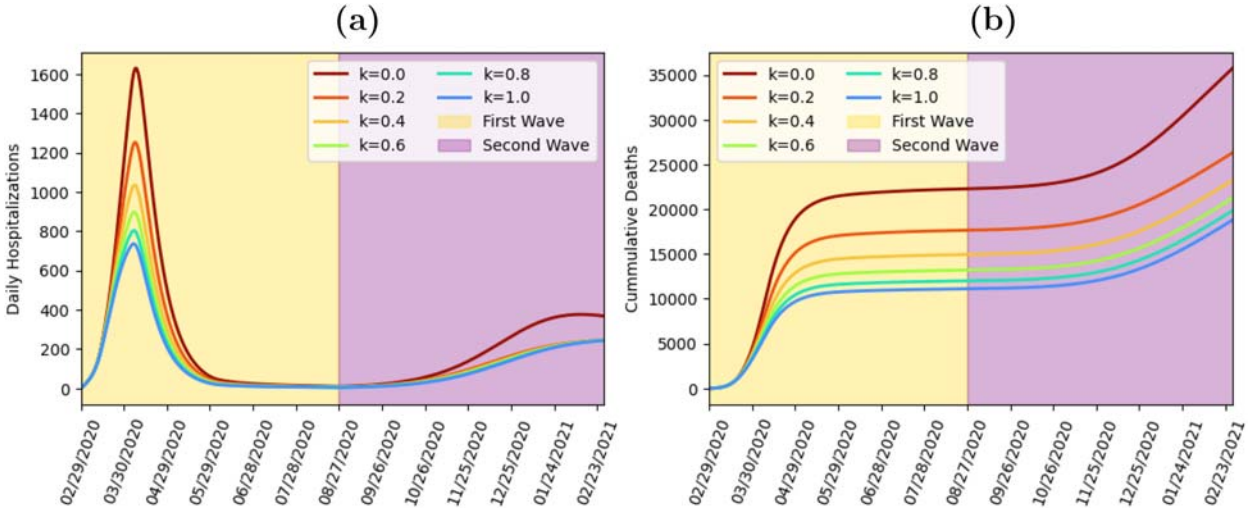

Fig. 15. Effect of initial sizes of the two behavioral groups on daily hospitalizations ($I_h(t)$) and cumulative mortality during the first two waves of the COVID-19 pandemic in New York City. Simulations of the 2-group behavior model (A.1) using the parameter values in Tables 3 and 4 and various initial sizes of the behavioral groups ($S_1(0) = kN(0)$ and $S_2(0) = (1-k)N(0)$, for $k = 0, 0.2, 0.4, \ldots, 1$). (a) Daily COVID-19 hospitalizations, as a function of time during the first two waves ($I_h(t)$). (b) Cumulative COVID-19 mortality, as a function of time during the first two waves in New York City.

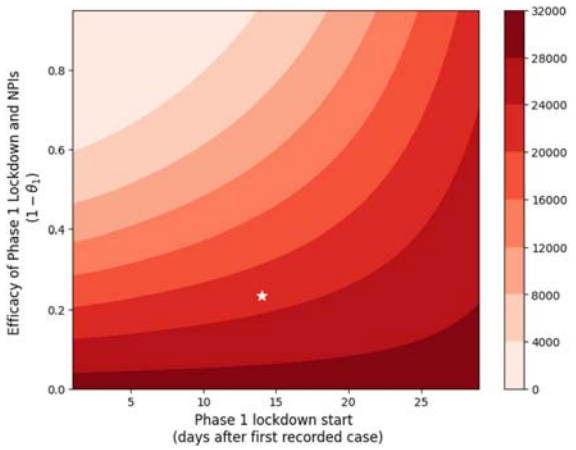

Fig. 16. Heat map assessing the effect of early implementation vs. efficacy of lockdown and other NPI measures ($1-\theta_{l,1}$) on the cumulative mortality during the first wave of the COVID-19 pandemic in New York City. Simulations of the 2-group behavior model (A.1) with the baseline values of the fixed and estimated parameters of the model given in Tables 3 and 4, respectively, and various values of $\theta_{l,1}$ and start dates for the implementation of the Phase 1 lockdown and other NPI measures after the index case of the COVID-19 pandemic in New York City. The white star marks the coordinates of the fitted value of $\theta_{l,1}=0.74664$ (estimated in Section 3.2.2) and the reported start date of lockdown in New York City (=14 days (Ferré-Sadurní, 2020)).

3.5.4. Impact of early implementation vs. efficacy of lockdown and other NPIs

In the previous sections, simulations of the model were carried out under the assumptions that Phase 1 of lockdown began in New York City 14 days after the index case of the COVID-19 pandemic was reported in the city and that the efficacy of lockdown and other NPIs during Phase 1 was somewhat low (approximately 25 %, as estimated in Section 3.2.2). It is instructive, therefore, to assess the population-level impact of varying the initial start date (beginning of Phase 1) and efficacy of the lockdown and other NPI measures (as measured by $1-\theta_{l,1}$) on the cumulative COVID-19 mortality at the end of the first wave in New York City. To achieve this objective, the 2-group behavior model (A.1) was simulated using the parameter values in Tables 3 and 4 and varying values of $1-\theta_{l,1}$ and the Phase 1 lockdown start date. The results, depicted by the heat map in Fig. 16, show a dramatic reduction in the cumulative COVID-19 mortality during the first wave with increasing efficacy of the intervention measures ($1-\theta_{l,1}$) even if the start date of the implementation of the intervention measures was up to the 14-day baseline. For instance, a 36 % reduction (from the baseline of 22,000 to 14,000) in the cumulative COVID-19 mortality can be recorded during the first wave if lockdown measures were implemented at the 14-day baseline period after the index case and the efficacy of this measure was 50 % (i.e., $1-\theta_{l,1}=0.5$). Furthermore, this heat map shows that if the lockdown and other NPI interventions were implemented earlier (e.g., five days after the index case), the COVID-19 pandemic would have been greatly suppressed in New York City if the efficacy of these interventions was at least 60 % (see the top-left corner of the heat map). This figure further shows a sizable increase in the first-wave cumulative mortality with increasing delay in the implementation of the intervention measures from the index case. If such delay is large enough, even high efficacy of these interventions only lead to a marginal reduction in cumulative mortality. For example, a 3-week delay in the implementation of these measures (after the index case) and 50 % efficacy will result in first wave cumulative mortality of about 20,000 (which represents only about 9 % reduction from the baseline value of 22,000). Furthermore, if the implementation is delayed by a month from the index case, even with the efficacy of these interventions as high as 90 %, up to 24,000 COVID-19 deaths would have be recorded by the end of the first wave in New York City (this represents a 10 % increase in the baseline cumulative mortality recorded). Overall, this figure emphasizes the importance of early implementation of lockdown and other NPI measures, at moderate to high efficacy levels, in successfully curtailing the burden of the COVID-19 pandemic in New York City during the first wave. In fact, no significant disease-induced mortality would have been recorded during the first wave of the COVID-19 pandemic if the lockdown and other NPI measures were implemented early (such as less than a week after the index case) and their efficacy was high enough (such as 60 %).

4. Discussion and conclusion

One of the key lessons learned during the COVID-19 pandemic was the impact of heterogeneity in changes in human behavior or attitudes towards the disease. Some of the notable heterogeneities in human behavior observed during the course of the pandemic include differences in attitude (i.e., acceptance, hesitancy, or refusal) towards the public health intervention and mitigation measures implemented in their community or jurisdiction (e.g., social distancing, quarantine, isolation, wearing a face mask in public, testing, and vaccination), acceptance and/or refusal of public health messaging and/or misinformation and disinformation and heterogeneities based on age, gender, race and political affiliation (or polarization) (Bir & Widmar, 2021; Lim et al., 2023; Stoler, 2022; Newman, 2020). This study is based on mathematical modeling, backed by data analytics and computation, to realistically quantify the impact of the aforementioned human behavioral changes and

heterogeneities on the spread and control of the COVID-19 pandemic in a population during the early stages of the pandemic. In particular, the study assessed the impacts of these heterogeneities during the first two waves of the pandemic in New York City (a one-time global epicenter of the pandemic, and the jurisdiction that suffered the most COVID-19 burden in the United States).

The objective of this study was achieved via the design, analysis, parameterization/validation, and simulations of a novel mechanistic mathematical model, which explicitly accounts for changes in human behavior during the pandemic by stratifying the total population into n behavioral groups based on their perception of risk (of acquisition/transmission of COVID-19 infection) and their resulting behavior choices with respect to the risk. Specifically, the first group (referred to as Group 1) represents individuals in the community who consistently adopt the most risk-averse behaviors against acquisition or transmission, while Groups 2 through n adopt increasing risk-taking behaviors as n increases (i.e., Group n is the most risk-tolerant behavior group in the community). The resulting behavior epidemic model, which takes the form of an n-group deterministic system of nonlinear differential equations, was rigorously analyzed for its basic qualitative properties (such as the invariance and non-negativity of its solutions).

A special case of the n-group model with two behavioral groups (i.e., $n = 2$), with one group for the most risk-averse and the other for the most risk-tolerant members of the community, was considered for mathematical tractability. The resulting 2-group behavior model was shown to have three nontrivial disease-free equilibria, namely, a cautious-only (risk-averse) disease-free equilibrium (denoted by G1DFE), a cautious-free (risk-tolerant) disease-free equilibrium (denoted by G2DFE), and a coexistence (where both risk-averse and risk-tolerant groups co-exist) disease-free equilibrium (denoted by G3DFE). These equilibria are shown to be stable whenever a certain epidemiological threshold, known as the control reproduction number (denoted by $\mathbb{R}_c$), is less than unity and the influence ratio (denoted by Γ) is greater, less than, or equal to 1, respectively. The epidemiological implication of this result is that, regardless of the value of the influence parameter Γ, no major outbreaks of the COVID-19 pandemic can occur in the community if the intervention and mitigation strategies implemented in the community are able to bring, and maintain, the control reproduction number to a value below unity. From a public health standpoint, the cautious-only equilibrium (G1DFE) is the most desirable, as it is associated with lower disease burden (as measured in terms of peak daily hospitalizations and cumulative mortality; see Table 8 and Fig. 15). It was further shown that, for the desirable G1DFE to be stable, it is necessary that $\Gamma = c_{12}^B/c_{21}^B$ must exceed unity (i.e., the risk-averse population must exert much higher level of influence on the non-cautious population than the other way round). While other studies have shown complementary results (for instance, Bir et al. (Bir & Widmar, 2021) shows that social influence in the form of the promotion of altruism is correlated with a higher likelihood of cautious behavior adoption, and Espinoza et al. (Espinoza et al., 2022) shows that the behavioral makeup of the population has a large impact on final epidemic size), the current study is among the first to highlight and rigorously show the major role that social (peer) influence plays on the dynamics of the COVID-19 pandemic, as measured in terms of helping to make the epidemiologically desirable disease-free equilibrium (G1DFE) to be stable.

The 2-group behavior model was calibrated using a 7-day running average of daily hospitalizations data (NYC Health, 2023) for the first wave of the COVID-19 pandemic in New York City (this corresponds to the time period from February 29th, 2020 to July 28th, 2020 (Centers for Disease Control, 2023)). The same hospitalizations dataset, for the period from July 29th, 2020 to March 25th, 2021, was used to cross-validate the calibrated 2-group behavior model, and the resulting fitted and cross-validated 2-group behavior model was used to estimate the eight unknown parameters of this model (and their associated 95 % confidence intervals were also given) and make predictions for the second wave of the COVID-19 pandemic in New York City. It was shown that, although the 2-group behavior model and its behavior-free equivalent (obtained by setting the behavior-related parameters of the 2-group behavior model to zero) fitted the first wave of the COVID-19 pandemic in New York City reasonably well, the behavior-free model failed to accurately predict the second wave, unlike the 2-group behavior model, which did so almost perfectly (see Figs. 6 and 10). This suggests that epidemic models of the COVID-19 pandemic that do not explicitly account for heterogeneous human behavior may fail to accurately predict the trajectory and burden of the pandemic in a population. This result complements the findings in (Pant et al., 2024; Venkatramanan et al., 2022).

Detailed global sensitivity analysis, in the form of PRCCs using Latin Hypercube Sampling (Blower & Dowlatabadi, 1994), was carried out for the 2-group behavior model to determine which of its 18 parameters had the largest impact on the two chosen response functions (namely, the peak daily COVID-19 hospitalizations and the cumulative mortality, corresponding to both the first and second waves of the COVID-19 pandemic in New York City). This analysis, carried out for two snapshots of time, namely April 20, 2020 (which corresponds to the middle of the first wave of the COVID-19 pandemic in New York City) and February 21, 2021 (which corresponds to the middle of the second wave of the pandemic in New York City), identified five main parameters of the 2-group behavior model that have the highest impact on the two response functions during the first two waves of the COVID-19 pandemic. The identified parameters were, the maximum effective contact rates for asymptomatically and symptomatically infectious individuals (β_a and β_i, respectively), the rate of progression of individuals leaving the exposed class (σ_e), and the parameter for the efficacy of the lockdown and other non-pharmaceutical interventions (NPIs) implemented during Phase 1 of the implementation period ($\theta_{l,1}$). The sensitivity analysis results suggest that the lockdown and NPI measures implemented would have significantly reduced the burden of the pandemic during the first two waves of

the pandemic in New York City (and, consequently, prevent the healthcare system from being overwhelmed during this period) if their efficacy and coverage was high enough (i.e., if the quantity, $1-\theta_{l,1}$, is high enough). This could be achieved by adequate preparation (such as stockpiling NPIs and making them widely available to the public) and early implementation of effective public health messaging campaigns encouraging adherence to intervention and mitigation measures against the pandemic.

The calibrated and validated 2-group behavior model was then simulated to quantify the impact of human behavioral changes and peer influence on the dynamics of the COVID-19 pandemic in New York City during the first two waves. In particular, two sets of numerical simulations were carried out to assess the impact of the behavioral parameters (namely, the hospitalization-motivated behavioral modification parameters, a_1 and a_2, and the influence-motivated behavioral modification parameters, c_{12}^B and c_{21}^B) on the burden of the pandemic in New York City during the first two waves. The first set of simulations was conducted by varying the hospitalization-motivated behavioral change parameters, a_1 and a_2, while fixing all other parameters of the behavior model with their baseline values (given in Tables 3 and 4). The results of these simulations showed that the first wave of the COVID-19 pandemic in New York City (as measured by the size of the peak daily hospitalizations and the cumulative COVID-19 mortality) was largely determined by the disease-motivated behavioral changes of individuals in Group 2 (the risk-tolerant group), while the impact of behavioral changes by risk-averse individuals (i.e., member of Group 1) was marginal during this time (i.e., the metrics for disease burden were more strongly correlated with changes in the parameter a_2, than with changes in the parameter a_1; see Fig. 13(a)). Hence, these simulations suggest that the first wave of the COVID-19 pandemic in New York City was largely driven by the behavior of the risk-tolerant group (as measured by changes in the parameter a_2), and much less so by the behavior of the risk-averse group; this may be due to the assumption that every member of the community started out in the risk-tolerant Group 1. Qualitatively similar results were obtained for the second wave, although the role of a_1 (i.e., its negative correlation with the disease burden) is more pronounced than it was during the first wave (see Fig. 13(b)). The simulations for the second wave also showed a threshold value of the parameter a_2, above which the cumulative COVID-19 mortality during this wave is minimized. In other words, this shows that if risk-tolerant individuals (i.e., members of Group 2) were to significantly decrease their contact rate in response to the level of hospitalizations in the community (i.e., if $a_2 > 2,200$, which roughly translates to a 40–80 % reduction of contacts at peak daily hospitalization times, see the orange curve in Fig. 2), the second wave of the COVID-19 pandemic in New York City would have been largely reduced or averted entirely.

Similar simulation results were obtained with respect to the disease burden by now varying the influence parameters, c_{12}^B and c_{21}^B, while keeping the hospitalization-induced behavior change parameters a_1 and a_2 (and all other parameters) fixed at their baseline values (given in Tables 3 and 4). In other words, this study showed that the size of the first wave of the COVID-19 pandemic in New York City (measured in terms of the peak daily hospitalizations and the cumulative COVID-19 mortality) was largely determined by the behavior of members of the risk-tolerant group (Group 2). In particular, the value of peak daily COVID-19 hospitalization is strongly affected by the average time taken by individuals in Group 2 to positively change their behavior (and move to the risk-averse Group 1) in response to peer pressure from members of Group 1 ($1/c_{12}^B$). For example, a 10-day reduction from the baseline value of this parameter (i.e.,from $1/c_{12}^B = 30$ days to 20 days) resulted in a 27 % reduction in peak daily hospitalization. Based on the data for the COVID-19 pandemic during the first wave in New York City (NYC Health, 2023), this will translate to a reduction of over 400 daily COVID-19-related hospitalizations (thereby significantly lessening the burden on the City's healthcare infrastructure). This suggests that a timely implementation of an effective public health strategy that emphasizes positive behavior changes due to social influences (i.e., decrease $1/c_{12}^B$, which can be achieved through, for example, positive messaging and advocacy from major community influencers, such as celebrities, community and religious leaders, and public health officials) will significantly decrease disease burden, as well as reduce strain on the healthcare system (Bir & Widmar, 2021; Parady et al., 2020; Viskupic & Wiltse, 2022).

Finally, simulations to assess the impact of relative behavioral group size at pandemic outset were carried out to determine to what extent the size of the disease burden was determined by the initial attitudes of members of the community (i.e., by members of groups 1 and 2) with respect to the disease risk. This was achieved by assuming a proportion, $k \in [0,1]$, of the initial number of susceptible individuals in the community started out as members of Group 1 (i.e., they initially started in the risk-averse group), while the remaining proportion, $1-k$, started out as members of Group 2 (i.e., they initially started in the risk-tolerant group). The simulations results obtained for this scenario (depicted in Fig. 15) showed a decrease in the peak daily hospitalizations and cumulative mortality with increasing values of k. Even a moderate increase in the baseline value of k (e.g., an increase from $k=0$ to $k=0.2$) reduced the baseline value of the peak daily hospitalizations by approximately 23 % during the first wave, and by 33 % during the second wave of the pandemic. This also decreased the cumulative mortality by approximately 22 % and 39 % by the end of the first and second waves, respectively (see Table 8). However, by separating these simulation results by pandemic waves (as shown in Figure C.3), it can be seen that this simple negative correlation between the value of k and the two disease metrics holds only for the first wave of the pandemic (see Figures C.3(a) and (c)), and not during the second. Specifically, for the second wave, this study showed that peak daily hospitalizations remained relatively constant (between 250 and 260 COVID-19 hospitalizations at the peak) regardless of the value of k (see Figure C.3(b)). For cumulative mortality of the second wave of the COVID-19 pandemic in New York City, simulations suggest that the impact of

increasing k changes depending on the size of k. For small values of k, (e.g. $0 < k < 0.1$) an increase in k within this interval is associated with a large *increase* in second wave cumulative mortality (see Figure C.3(d)). This is likely due to the corresponding increase in the length of the second wave as k increases in the interval (0, 0.1) (see Figure C.5 in Appendix C). However, for values of k larger than 0.1, an increase in k leads to a decrease in second wave cumulative mortality (see Figure C.3(d)). This suggests that having a significant proportion of members of the community starting out in the risk-averse group (e.g., $k > 0.2$) at the beginning of the COVID-19 pandemic will lead to a much smaller pandemic overall in New York City. These results, combined with the earlier simulation results, support the conclusion that a risk-averse attitude at the early stages of the pandemic, coupled with early implementation of effective public health intervention and mitigation measures, are vital for effectively combating, suppressing or eliminating the burden of respiratory pandemics, such as the COVID-19 pandemic.

Although the n-group behavior model considered in this study incorporated many key pertinent features of the COVID-19 pandemic, it is not without some limitations. For instance, since peer influence changes over time in reality, the model may be improved by relaxing the assumption that the peer influence parameters (c_{ij}^B, with $i, j = 1, 2, \ldots, n$ and $i \neq j$) are constant (i.e., re-defining the rates c_{ij}^B to be functions of time, thereby making the model to be non-autonomous (Gumel, Iboi, Ngonghala, & Elbasha, 2021; Munoz-Fernandez et al., 2021; Pei & Zhang, 2022)). The model may further be improved by explicitly incorporating related heterogeneities, such as age, sex, race, political affiliation, and socio-economic status. The authors hope to consider these options in a future study (Arthur et al., 2021; Pisaneschi et al., 2024; Saad-Roy & Traulsen, 2023). Finally, the 2-group behavior model considered in this study was calibrated using disease data to estimate its unknown epidemiological and behavioral parameters (although the values of the behavioral change parameters a_1 and a_2 were verified using mask compliance data from the New York City subway system, available starting mid June 2020 (MTA subway and bus mask, 2024; see Fig. 9). However, it would have been ideal to parameterize the behavior-related parameters of the model with human behavior data, which, unfortunately, was not available (for New York City during the first two waves of the pandemic) until several months after the advent of the pandemic. This study, therefore, strongly highlights the need for the collection of such behavior-related data (for risk-taking and adherence to interventions) during the early stages of major respiratory pandemics, and making such data publicly available for modelers to use. Such crucially important data can be collected using surveys and digital tools (such as computer vision to determine how many people are wearing masks (MTA subway and bus mask, 2024)). Behavioral data can also be collected through mobile phone data (Cowley et al., 2021) or well-done contact surveys (Chin et al. 2024). Overall, this study shows that the prospect of the effective control of the COVID-19 pandemic in a large population stratified by human behavior changes using NPIs (if implemented in an effective and timely manner) is highly promising.

CRediT authorship contribution statement

Alice Oveson: Writing – original draft, Visualization, Validation, Methodology, Investigation, Formal analysis, Conceptualization. **Michelle Girvan:** Writing – original draft, Methodology, Conceptualization. **Abba B. Gumel:** Writing – original draft, Supervision, Project administration, Methodology, Investigation, Funding acquisition, Formal analysis, Conceptualization.

Declaration of competing interests

The author is an Editorial Board Member/Editor-in-Chief/Associate Editor/Guest Editor for Infectious Disease Modelling and was not involved in the editorial review or the decision to publish this article.

Acknowledgments

ABG acknowledges the support, in part, of the National Science Foundation (Grant Number: DMS-2052363; transferred to DMS-2330801). AO acknowledges the support of the University of Maryland School of Graduate Studies Dean's Fellowship. The authors are grateful to the two anonymous reviewers for their very constructive comments, which enhanced the clarity of the manuscript.

Appendices

A Equations for Special Cases of the n-group Behavior Model (2.1)

A.1 Equations for the special case with $n = 2$

Setting $n = 2$ in the behavior model (A.1) gives the following 2-group behavior model for COVID-19 dynamics:

$$
\begin{aligned}
\dot{S_1}(t) =\ & \xi R_1(t) - \theta_l \left[\frac{c_1^A(t)S_1(t)}{N(t)}\right] \sum_{j=1}^{2} c_j^A(t)\left[\beta_a I_{a,j}(t) + \beta_i I_{s,j}(t) + \beta_h I_{h,j}(t)\right] \\
& + c_{12}^B \frac{S_2(t)N_1(t)}{N(t)} - c_{21}^B \frac{S_1(t)N_2(t)}{N(t)}, \\
\dot{S_2}(t) =\ & \xi R_2(t) - \theta_l \left[\frac{c_2^A(t)S_2(t)}{N(t)}\right] \sum_{j=1}^{2} c_j^A(t)\left[\beta_a I_{a,j}(t) + \beta_i I_{s,j}(t) + \beta_h I_{h,j}(t)\right] \\
& + c_{21}^B \frac{S_1(t)N_2(t)}{N(t)} - c_{12}^B \frac{S_2(t)N_1(t)}{N(t)}, \\
\dot{E}_1(t) =\ & \theta_l \left[\frac{c_1^A(t)S_1(t)}{N(t)}\right] \sum_{j=1}^{2} c_j^A(t)\left[\beta_a I_{a,j}(t) + \beta_i I_{s,j}(t) + \beta_h I_{h,j}(t)\right] - \sigma_e E_1(t) \\
& + c_{12}^B \frac{E_2(t)N_1(t)}{N(t)} - c_{21}^B \frac{E_1(t)N_2(t)}{N(t)}, \\
\dot{E}_2(t) =\ & \theta_l \left[\frac{c_2^A(t)S_2(t)}{N(t)}\right] \sum_{j=1}^{2} c_j^A(t)\left[\beta_a I_{a,j}(t) + \beta_i I_{s,j}(t) + \beta_h I_{h,j}(t)\right] - \sigma_e E_2(t) \\
& + c_{21}^B \frac{E_1(t)N_2(t)}{N(t)} - c_{12}^B \frac{E_2(t)N_1(t)}{N(t)},
\end{aligned} \tag{A.1}
$$

$$
\begin{aligned}
\dot{I}_{a,1}(t) =& (1-r)\sigma_e E_1(t) - \gamma_a I_{a,1}(t) + c_{12}^B \frac{I_{a,2}(t)N_1(t)}{N(t)} - c_{21}^B \frac{I_{a,1}(t)N_2(t)}{N(t)}, \\
\dot{I}_{a,2}(t) =& (1-r)\sigma_e E_2(t) - \gamma_a I_{a,2}(t) + c_{21}^B \frac{I_{a,1}(t)N_2(t)}{N(t)} - c_{12}^B \frac{I_{a,2}(t)N_1(t)}{N(t)}, \\
\dot{I}_{s,1}(t) =& r\sigma_e E_1(t) - \sigma_i I_{s,1}(t) + c_{12}^B \frac{I_{s,2}(t)N_1(t)}{N(t)} - c_{21}^B \frac{I_{s,1}(t)N_2(t)}{N(t)}, \\
\dot{I}_{s,2}(t) =& r\sigma_e E_2(t) - \sigma_i I_{s,2}(t) + c_{21}^B \frac{I_{s,1}(t)N_2(t)}{N(t)} - c_{12}^B \frac{I_{s,2}(t)N_1(t)}{N(t)}, \\
\dot{I}_{h,1}(t) =& q\sigma_i I_{s,1}(t) - (\gamma_h + \delta_h) I_{h,1}(t) + c_{12}^B \frac{I_{h,2}(t)N_1(t)}{N(t)} - c_{21}^B \frac{I_{h,1}(t)N_2(t)}{N(t)}, \\
\dot{I}_{h,2}(t) =& q\sigma_i I_{s,2}(t) - (\gamma_h + \delta_h) I_{h,2}(t) + c_{21}^B \frac{I_{h,1}(t)N_2(t)}{N(t)} - c_{12}^B \frac{I_{h,2}(t)N_1(t)}{N(t)}, \\
\dot{R_1}(t) =& \gamma_a I_{a,1}(t) + (1-q)\sigma_i I_{s,1}(t) + \gamma_h I_{h,1}(t) - \xi R_1(t) + c_{12}^B \frac{R_2(t)N_1(t)}{N(t)} - c_{21}^B \frac{R_1(t)N_2(t)}{N(t)}, \\
\dot{R_2}(t) =& \gamma_a I_{a,2}(t) + (1-q)\sigma_i I_{s,2}(t) + \gamma_h I_{h,2}(t) - \xi R_2(t) + c_{21}^B \frac{R_1(t)N_2(t)}{N(t)} - c_{12}^B \frac{R_2(t)N_1(t)}{N(t)}.
\end{aligned}
$$

A.2 Equations for the behavior-free version of the 2-group model (A.1)

Define $S(t) = S_1(t) + S_2(t)$, $E(t) = E_1(t) + E_2(t)$, $I_a(t) = I_{a,1}(t) + I_{a,2}(t)$, $I_s(t) = I_{s,1}(t) + I_{s,2}(t)$, $I_h(t) = I_{h,1}(t) + I_{h,2}(t)$, and $R(t) = R_1(t) + R_2(t)$. Substituting these expressions into the 2-group model (A.1), and setting the behavior-related parameters (a_1, a_2, c_{12}^B, and c_{21}^B) to zero, gives the following behavior-free version of the 2-group model (A.1) gives

$$
\begin{aligned}
\dot{S}(t) &= \xi R_1(t) - \theta_l \frac{S(t)}{N(t)}(\beta_a I_a(t) + \beta_i I_s(t) + \beta_h I_h(t)),\\
\dot{E}(t) &= \theta_l \frac{S(t)}{N(t)}(\beta_a I_a(t) + \beta_i I_s(t) + \beta_h I_h(t)) - \sigma_e E(t),\\
\dot{I}_a(t) &= (1-r)\sigma_e E(t) - \gamma_a I_a(t),\\
\dot{I}_s(t) &= r\sigma_e E(t) - \sigma_i I_s(t),\\
\dot{I}_h(t) &= q\sigma_i I_s(t) - (\gamma_h + \delta_h) I_h(t),\\
\dot{R}(t) &= \gamma_a I_a(t) + (1-q)\sigma_i I_s(t) + \gamma_h I_h(t) - \xi R(t).
\end{aligned}
\tag{A.2}
$$

B Proof of Theorem 3.4

Proof. The proof of Theorem 3.4 is based on linearizing the 2-group behavior model (A.1) around the G1DFE and taking advantage of the properties of Metzler matrices as described in (Kamgang & Sallet, 2008). It is convenient to reorder the equations of the 2-group model (A.1) such that the equations corresponding to the non-disease (i.e., susceptible and recovered) compartments (S_1, S_2, R_1 and R_2) are first, followed by the equations corresponding to the eight infected compartments (E_1, E_2, $I_{a,1}$, $I_{a,2}$, …, $I_{h,2}$). The Jacobian of the reordered system, evaluated at the G1DFE, is given by the following block upper triangular matrix:

$$
J|_{G1DFE} = \begin{bmatrix} A_{11} & A_{12} \\ \mathbf{0}_{8\times 4} & A_{22} \end{bmatrix},
$$

where

$$
A_{11} = \begin{bmatrix}
0 & c_{12}^B - c_{21}^B & \xi & -c_{21}^B \\
0 & c_{21}^B - c_{12}^B & 0 & c_{21}^B + \xi \\
0 & 0 & -\xi & c_{12}^B \\
0 & 0 & 0 & -c_{12}^B - \xi
\end{bmatrix},
\tag{B.1}
$$

$$
A_{22} = \begin{bmatrix}
-\sigma_e & c_{12}^B & \beta_a\theta_l & \beta_a\theta_l & \beta_i\theta_l & \beta_i\theta_l & \beta_h\theta_l & \beta_h\theta_l \\
0 & -c_{12}^B - \sigma_e & 0 & 0 & 0 & 0 & 0 & 0 \\
(1-r)\sigma_e & 0 & -\gamma_a & c_{12}^B & 0 & 0 & 0 & 0 \\
0 & (1-r)\sigma_e & 0 & -c_{12}^B - \gamma_a & 0 & 0 & 0 & 0 \\
r\sigma_e & 0 & 0 & 0 & -\sigma_i & c_{12}^B & 0 & 0 \\
0 & r\sigma_e & 0 & 0 & 0 & -c_{12}^B - \sigma_i & 0 & 0 \\
0 & 0 & 0 & 0 & q\sigma_i & 0 & -\delta_h - \gamma_h & c_{12}^B \\
0 & 0 & 0 & 0 & 0 & q\sigma_i & 0 & -c_{12}^B - \delta_h - \gamma_h
\end{bmatrix},
\tag{B.2}
$$

and $\mathbf{0}_{8\times 4}$ is an eight by four zero matrix. The matrix A_{12} is the 4×8 matrix corresponding to the derivatives of the non-disease compartments (S_1, S_2, R_1 and R_2) with respect to the eight disease compartments (E_1, E_2, $I_{a,1}$, $I_{a,2}$, …, $I_{h,2}$) evaluated at G1DFE. Since the matrix A_{12} is not relevant in the computation of the eigenvalues of $J|_{G1DFE}$, it is not explicitly defined or given here. The eigenvalues of the block upper triangular matrix $J|_{G1DFE}$ are the eigenvalues of its diagonal blocks (A_{11} and A_{22}). It can be seen that the eigenvalues of the matrix A_{11} are:

$$
\sigma(A_{11}) = \{0, c_{21}^B - c_{12}^B, -\xi, -c_{12}^B - \xi\},
$$

from which it follows that three of the four eigenvalues of the matrix A_{11} are negative (with one eigenvalue being identically equal to zero) provided that the following inequality is satisfied:

$$\text{Condition 1: } c_{12}^B > c_{21}^B. \tag{B.3}$$

Unlike in the case of the matrix A_{11}, the eigenvalues of the matrix A_{22} cannot be readily computed directly. The eigenvalues of the matrix A_{22} will be obtained using the properties of Metzler stable matrices (recall that a Metzler stable matrix is a Metzler matrix with all its eigenvalues having negative real part (Kamgang & Sallet, 2008)). This will be achieved by using Proposition 3.1 of (Kamgang & Sallet, 2008).

Proposition B.1. (*Proposition* 3.1 *of* (Kamgang & Sallet, 2008)) *Let M be a Metzler matrix, which is block decomposed*:

$$M = \begin{bmatrix} A & B \\ C & D \end{bmatrix},$$

where A and D are square matrices. Then M is Metzler stable if and only if A and $D - CA^{-1}B$ are Metzler stable.

To apply this method, A_{22} is broken down into smaller (and more tractable) matrices. Specifically, this is done by re-writing A_{22} as:

$$A_{22} = \begin{bmatrix} P & Q \\ R & S \end{bmatrix},$$

where

$$P = \begin{bmatrix} -\sigma_e & c_{12}^B & \beta_a\theta_l & \beta_a\theta_l \\ 0 & -c_{12}^B - \sigma_e & 0 & 0 \\ \sigma_e(1-r) & 0 & -\gamma_a & c_{12}^B \\ 0 & \sigma_e(1-r) & 0 & -c_{12}^B - \gamma_a \end{bmatrix}, Q = \begin{bmatrix} \beta_i\theta_l & \beta_i\theta_l & \beta_h\theta_l & \beta_h\theta_l \\ 0 & 0 & 0 & 0 \\ 0 & 0 & 0 & 0 \\ 0 & 0 & 0 & 0 \end{bmatrix} \tag{B.4}$$

$$R = \begin{bmatrix} r\sigma_e & 0 & 0 & 0 \\ 0 & r\sigma_e & 0 & 0 \\ 0 & 0 & 0 & 0 \\ 0 & 0 & 0 & 0 \end{bmatrix}, S = \begin{bmatrix} -\sigma_i & c_{12}^B & 0 & 0 \\ 0 & -c_{12}^B - \sigma_i & 0 & 0 \\ q\sigma_i & 0 & -\delta_h - \gamma_h & c_{12}^B \\ 0 & q\sigma_i & 0 & -c_{12}^B - \delta_h - \gamma_h \end{bmatrix}. \tag{B.5}$$

From Proposition 3.1 of (Kamgang & Sallet, 2008), the matrix A_{22} is Metzler stable if and only if the matrices P and $S - RP^{-1}Q$ are Metzler stable. As a principal sub-matrix of a Metzler matrix, P is clearly a Metzler matrix (Kamgang & Sallet, 2008). To confirm the Metzler stability of P, it is necessary to compute its eigenvalues, which are given by:

$$\sigma(P) = \left\{ -c_{12}^B - \gamma_a, -c_{12}^B - \sigma_e, -\frac{\gamma_a + \sigma_e}{2} \pm \lambda_P \right\},$$

where

$$\lambda_P = \frac{1}{2}\sqrt{(\gamma_a - \sigma_e)^2 + 4(1-r)\beta_a\sigma_e\theta_l},$$

from which it follows that all eigenvalues of P are strictly negative (making P Metzler stable) if and only if the following condition is satisfied:

$$\text{Condition 2: } \frac{(1-r)\beta_a\theta_l}{\gamma_a} < 1. \tag{B.6}$$

Hence, if Condition 2 holds, the matrix P is Metzler stable. The next step is to compute the matrix $S - RP^{-1}Q$:

$$S - RP^{-1}Q = \begin{bmatrix} \frac{\beta_i\gamma_a r\theta_l}{\gamma_a-(1-r)\beta_a\theta_l} - \sigma_i & c_{12}^B + \frac{\beta_i\gamma_a r\theta_l}{\gamma_a-(1-r)\beta_a\theta_l} & \frac{\beta_h\gamma_a r\theta_l}{\gamma_a-(1-r)\beta_a\theta_l} & \frac{\beta_h\gamma_a r\theta_l}{\gamma_a-(1-r)\beta_a\theta_l} \\ 0 & -c_{12}^B - \sigma_i & 0 & 0 \\ q\sigma_i & 0 & -\delta_h - \gamma_h & c_{12}^B \\ 0 & q\sigma_i & 0 & -c_{12}^B - \delta_h - \gamma_h \end{bmatrix}. \tag{B.7}$$

It follows that, if Condition 2 holds, then $S - RP^{-1}Q$ is a Metzler matrix, but its eigenvalues are not easily computed. Proposition 3.1 of (Kamgang & Sallet, 2008) can be applied to the Metzler matrix $S - RP^{-1}Q$ to enable the computation of its eigenvalues based (on computing the eigenvalues for a simpler two by two matrix), as follows:

$$S - RP^{-1}Q = \begin{bmatrix} W & X \\ Y & Z \end{bmatrix},$$

where

$$W = \begin{bmatrix} \frac{\beta_i\gamma_a r\theta_l}{\gamma_a-(1-r)\beta_a\theta_l} - \sigma_i & c_{12}^B + \frac{\beta_i\gamma_a r\theta_l}{\gamma_a-(1-r)\beta_a\theta_l} \\ 0 & -c_{12}^B - \sigma_i \end{bmatrix}, X = \begin{bmatrix} \frac{\beta_h\gamma_a r\theta_l}{\gamma_a-(1-r)\beta_a\theta_l} & \frac{\beta_h\gamma_a r\theta_l}{\gamma_a-(1-r)\beta_a\theta_l} \\ 0 & 0 \end{bmatrix}, \tag{B.8}$$

$$Y = \begin{bmatrix} q\sigma_i & 0 \\ 0 & q\sigma_i \end{bmatrix}, \; Z = \begin{bmatrix} -\delta_h - \gamma_h & c_{12}^B \\ 0 & -c_{12}^B - \delta_h - \gamma_h \end{bmatrix}, \tag{B.9}$$

from which it follows that the matrix $S - RP^{-1}Q$ will be Metzler stable if and only if the matrices W and $Z - YW^{-1}X$ are Metzler stable. The matrix W is a principal sub-matrix of a Metzler matrix. Hence, it is a Metzler matrix, and its eigenvalues are given by:

$$\sigma(W) = \left\{ \frac{\beta_i\gamma_a r\theta_l}{\gamma_a-(1-r)\beta_a\theta_l} - \sigma_i, -c_{12}^B - \sigma_i \right\},$$

which are strictly negative if the following condition holds:

$$\text{Condition 3: } \frac{r\beta_i\theta_l}{\sigma_i} + \frac{(1-r)\beta_a\theta_l}{\gamma_a} < 1 \tag{B.10}$$

If Condition 3 holds, then the matrix W is Metzler stable. We have

$$Z - YW^{-1}X = \begin{bmatrix} \frac{\beta_h\gamma_a rq\sigma_i\theta_l}{-\beta_i\gamma_a r\theta_l + \sigma_i(\gamma_a-(1-r)\beta_a\theta_l)} - \gamma_h - \delta_h & c_{12}^B + \frac{\beta_h\gamma_a rq\sigma_i\theta_l}{-\beta_i\gamma_a r\theta_l + \sigma_i(\gamma_a-(1-r)\beta_a\theta_l)} \\ 0 & -c_{12}^B - \delta_h - \gamma_h \end{bmatrix}. \tag{B.11}$$

To prove that $Z - YW^{-1}X$ is a Metzler matrix, the following inequality must hold:

$$c_{12}^B + \frac{\beta_h\gamma_a rq\sigma_i\theta_l}{-\beta_i\gamma_a r\theta_l + \sigma_i(\gamma_a-(1-r)\beta_a\theta_l)} > 0. \tag{B.12}$$

Given the positivity of the parameters $c_{12}^B, \beta_h, \gamma_a, r, q, \sigma_i$ and θ_l, the above inequality holds whenever the following simplified inequality holds.

$$-\beta_i\gamma_a r\theta_l + \sigma_i(\gamma_a-(1-r)\beta_a\theta_l) > 0, \tag{B.13}$$

which follows directly from Condition 3 above. Hence, $Z - YW^{-1}X$ is a Metzler matrix. To prove that this matrix is Metzler stable, consider its eigenvalues, which are given by:

$$\sigma(Z - YW^{-1}X) = \left\{ \frac{\beta_h\gamma_a rq\sigma_i\theta_l}{\gamma_a\sigma_i - \beta_a\sigma_i\theta_l - \beta_i\gamma_a r\theta_l + \beta_a r\sigma_i\theta_l} - \gamma_h - \delta_h, -c_{12}^B - \delta_h - \gamma_h \right\}.$$

These eigenvalues will be strictly negative if the following condition holds:

$$\text{Condition 4: } \theta_I\left(\frac{\beta_h r q}{\gamma_h+\delta_h}+\frac{(1-r)\beta_a}{\gamma_a}+\frac{r\beta_i}{\sigma_i}\right)=\mathbb{R}_c<1. \tag{B.14}$$

Hence, if Condition 4 holds, the matrix $Z-YW^{-1}X$ is Metzler stable. This (in conjunction with the Metzler stability of the matrix W) implies that the matrix $S-RP^{-1}Q$ is Metzler stable, which implies that, if Conditions 1 through 4 hold, the matrix A_{22} is Metzler stable. Thus, all eigenvalues of the matrix A_{22} have negative real parts. Furthermore, it should be noted that Condition 4 also contains Conditions 2 and 3. Thus, if Conditions 1 and 4 hold, the matrix A_{22} is Metzler stable. Furthermore, the eigenvalues of the Jacobian matrix evaluated at G1DFE are given by the union of the eigenvalues of A_{11} and A_{22}. That is,

$$\sigma(J|_{G1DFE})=\sigma(A_{11})\cup\sigma(A_{22}).$$

Thus, if Conditions 1 and 4 hold, the matrix A_{22} is Metzler stable (meaning its eigenvalues have negative real parts) and the matrix A_{11} has three eigenvalues with negative real parts and one eigenvalue identically equal to zero, so 11 of the 12 eigenvalues of the Jacobian $J|_{G1DFE}$ of the behavior model (A.1) evaluated around the G1DFE have negative real parts, and the remaining eigenvalue is identically zero. Hence, the G1DFE is marginally stable (Strogatz, 2024) whenever Conditions 1 (i.e., $c_{12}^B>c_{21}^B$) and 4 (i.e., $\mathbb{R}_c<1$) hold. □

C Additional Simulation Figures and Tables

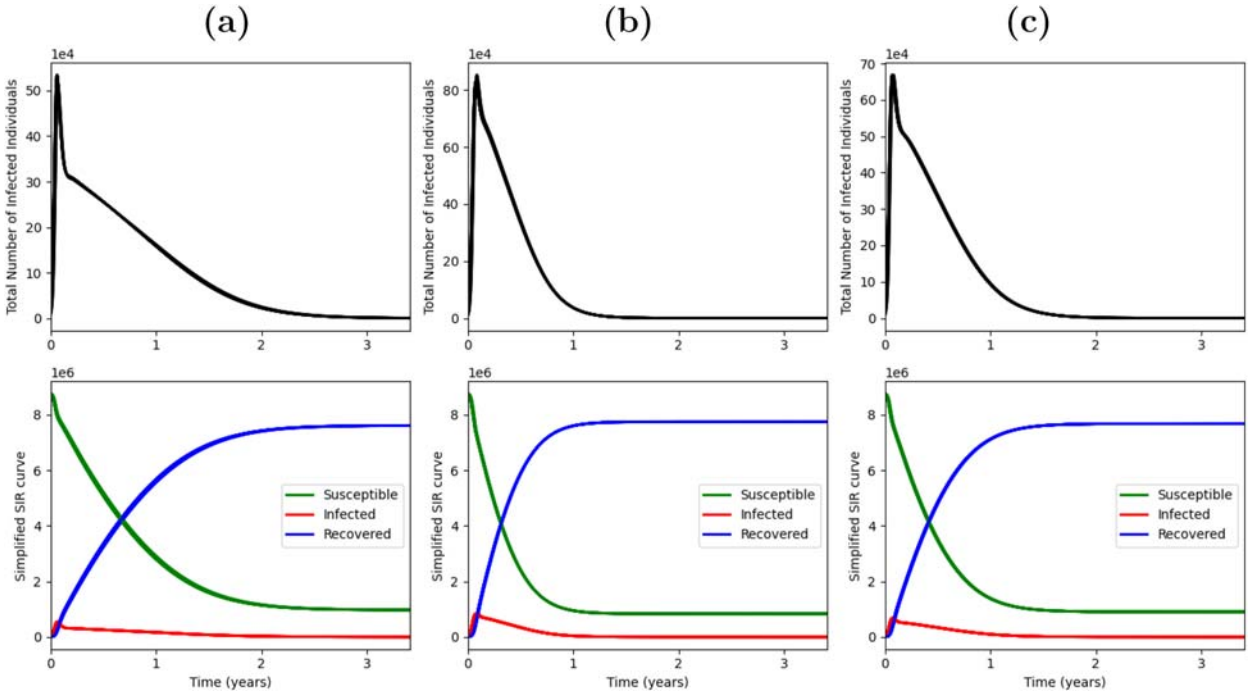

Fig. C.1. Simulations of the 2-group model (A.1), showing the profile of the total number of infected individuals (top) and the total number of individuals in the community, stratified by disease state (susceptible, infected, recovered), as a function of time for various initial conditions. Column (a): $c_{12}^B=0.5, c_{21}^B=0.25$ ($\Gamma=2>1$). Column (b): $c_{12}^B=0.25, c_{21}^B=0.5$ ($\Gamma=0.5<1$). Column (c): $c_{12}^B=c_{21}^B=0.5$ ($\Gamma=1$). In all panels all other parameter values used in these simulations are as given in Tables 3 and 4, but with $\theta_l=1$, $\beta_a=1$, $\beta_i=0.5$, and $\xi=0$ (so that, $\mathbb{R}_c=7.8>1$ and infection does not induce permanent immunity). These simulations show that when $\mathbb{R}_c>1$ and infection does not induce permanent immunity, solutions of the 2-group model (A.1) satisfy the Kermack-Mckendrick constraint $S(\infty)-S(0)>0$ (Gumel, Iboi, Ngonghala, & Elbasha, 2021), regardless of the value of Γ.

Table 9
Baseline values and ranges for the 18 parameters of the 2-group behavior model (A.1). The baseline values are as given in Tables 3 and 4, and the range of each parameter is determined by taking 40 % to the left and right of its baseline value (Blower & Dowlatabadi, 1994; Marino et al., 2008; McLeod et al., 2006).

Parameter	Baseline value	Range
$\theta_{l,1}$	0.74664 (dimensionless)	[0.448,1.045]
$\theta_{l,2}$	0.00133 (dimensionless)	[0.0008,0.0019]
$\theta_{l,3}$	0.15427 (dimensionless)	[0.0926,0.216]

Table 9 (*continued*)

Parameter	Baseline value	Range
$\theta_{l,4}$	0.30970 (dimensionless)	[0.186,0.434]
c_{12}^B	1/30 day^{-1}	[0.02,0.0467]
c_{21}^B	1/90 day^{-1}	[0.00667,0.0156]
a_1	8000 (dimensionless)	[4,800,11,200]
a_2	2800 (dimensionless)	[1,680,3920]
Ξ	1/180 day^{-1}	[0.00333,0.00778]
σ_i	1/14 day^{-1}	[0.0429,0.1]
σ_e	0.25 day^{-1}	[0.15,0.35]
γ_a	1/9 day^{-1}	[0.0667,0.1556]
γ_h	0.1 day^{-1}	[0.06,0.14]
δ_h	0.41 day^{-1}	[0.246,0.574]
β_a	0.625 day^{-1}	[0.375,0.875]
β_i	0.375 day^{-1}	[0.225,0.525]
R	0.6 (dimensionless)	[0.36,0.84]
q	0.05 (dimensionless)	[0.03,0.07]

Table 10
Partial rank correlation coefficients (PRCCs) of the 18 parameters of the 2-group behavior model (A.1) at two time periods (April 2020 and February 2021) during the COVID-19 pandemic in New York City, with respect to: (a) peak daily COVID-19 hospitalizations and (b) cumulative COVID-19 mortality. The baseline values and ranges of the parameters used in generating the PRCC values are given in Table 9.

(a)

Parameter	Apr 2020	Feb 2021
$\theta_{l,1}$	0.806	0.262
$\theta_{l,2}$	0.165	0.0277
$\theta_{l,3}$	−0.0524	0.241
$\theta_{l,4}$	0.0670	0.744
c_{12}^B	−0.261	−0.228
c_{21}^B	−0.00475	−0.00195
a_1	0.0285	0.0147
a_2	−0.185	−0.152
ξ	0.188	0.0897
σ_i	−0.125	−0.864
σ_e	0.786	−0.0545
γ_a	−0.448	−0.711
γ_h	−0.104	−0.187
δ_h	−0.612	−0.0580
β_a	0.849	0.561
β_i	0.842	0.535
r	−0.130	−0.290
q	0.576	−0.041

(b)

$\theta_{l,1}$	0.665	0.661
$\theta_{l,2}$	−0.102	0.0156
$\theta_{l,3}$	−0.0616	0.305
$\theta_{l,4}$	0.138	0.572
c_{12}^B	0.0266	−0.152
c_{21}^B	−0.0396	−0.125
a_1	−0.169	−0.127
a_2	−0.126	−0.141
ξ	−0.0535	0.0738
σ_i	0.160	−0.778
σ_e	0.796	0.470
γ_a	−0.268	−0.539
γ_h	−0.167	0.127
δ_h	0.518	0.436
β_a	0.772	0.606
β_i	0.785	0.691
R	0.343	0.0223
Q	0.690	0.219

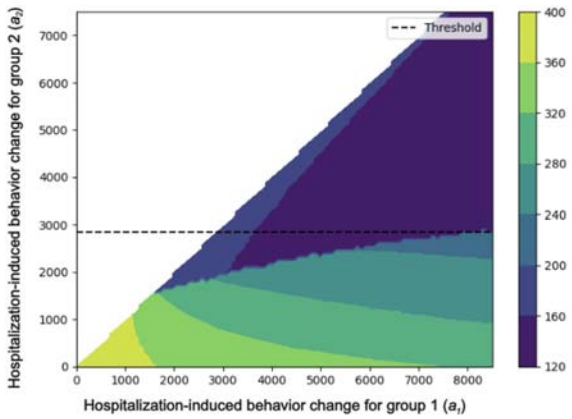

Fig. C.2. Effect of the hospitalization-motivated behavioral modifiers, a_1 and a_2, on the length (in days) of the second wave of the COVID-19 pandemic in New York City. Simulations of the model (A.1) with the baseline parameter values in Tables 3 and 4, and various values of a_1 and a_2. The end of the second wave was determined by the first day of the simulation after the start of the second wave wherein the total number of infected individuals (including exposed, asymptomatically infectious, symptomatically infectious, and hospitalized individuals) fell below 200.

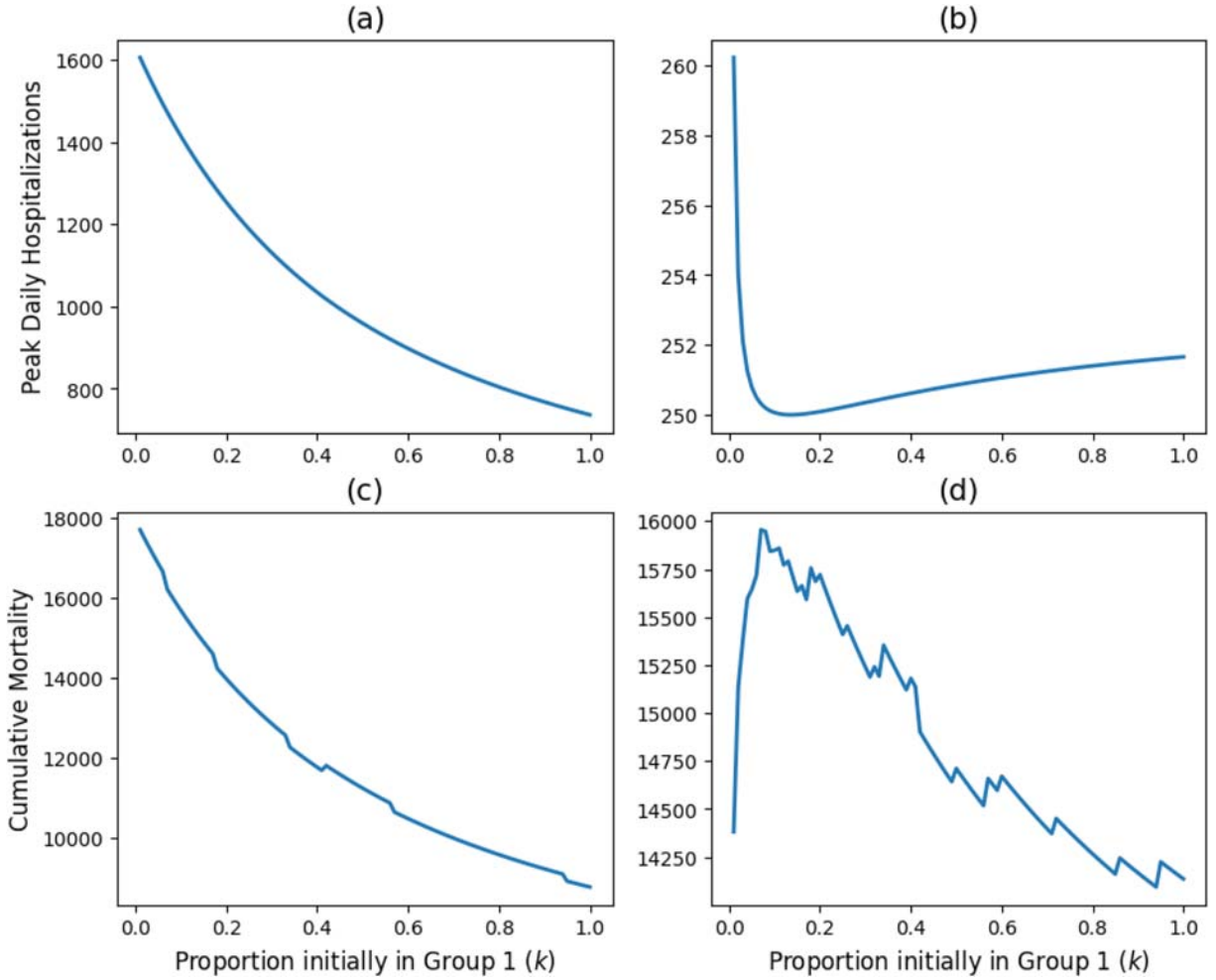

Fig. C.3. Effect of initial sizes of the two behavioral groups on peak daily hospitalizations and cumulative mortality during the first two waves of the COVID-19 pandemic in New York City. Simulations of the behavior model (A.1) using the parameter values in Tables 3 and 4 and various initial sizes of the behavioral groups ($S_1(0) = kN(0)$ and $S_2(0) = (1-k)N(0)$, for $k = 0, 0.2, 0.4, \ldots, 1$). (a) First wave peak daily hospitalizations, as a function of initial Group 1 size (k). (b) Second wave peak daily hospitalizations, as a function of initial Group 1 size (k). (c) First wave cumulative mortality, as a function of initial Group 1 size (k). (d) Second wave cumulative mortality, as a function of initial Group 1 size (k).

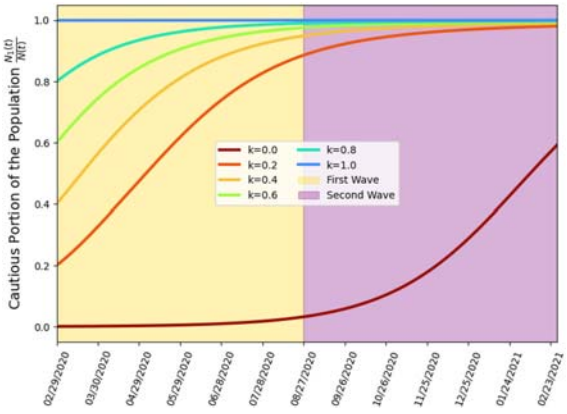

Fig. C.4. Effect of initial sizes of the two behavioral groups on the relative size of Group 1 ($\frac{N_1(t)}{N(t)}$) during the first two waves of the COVID-19 pandemic in New York City. Simulations of the 2-group behavior model (A.1) using the parameter values in Tables 3 and 4 and various initial sizes of the behavioral groups ($S_1(0) = kN(0)$ and $S_2(0) = (1 - k)N(0)$, for $k = 0, 0.2, 0.4, \ldots, 1$).

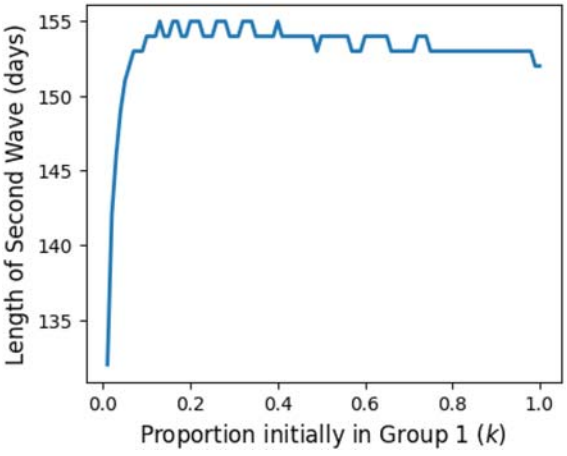

Fig. C.5. Effect of initial sizes of the behavioral groups on the length (in days) of the second wave of the COVID-19 pandemic in New York City. Simulations of the model (A.1) with the baseline parameter values in Tables 3 and 4 and various initial sizes of behavioral groups ($S_1(0) = kN(0)$ and $S_2(0) = (1 - k)N(0)$ for $0 \leq k \leq 1$). The end of the second wave was determined by the first day of the simulation after the start of the second wave wherein the total number of infected individuals (including exposed, asymptomatically infectious, symptomatically infectious, and hospitalized individuals) fell below 200.

References

Akaike, H. (1974). A new look at the statistical model identification. *IEEE Transactions on Automatic Control, 19*(6).
Altman, J. D., Miner, D. S., Lee, A. A., Asay, A. E., Nielson, B. U., et al. (2023). Factors affecting vaccine attitudes influenced by the COVID-19 pandemic. *Vaccines, 11*(3).
Amid ongoing COVID-19 pandemic. (2020). Governor Cuomo announces New York City playgrounds will close. Available at: https://www.governor.ny.gov/news/video-audio-rush-transcript-amid-ongoing-covid-19-pandemic-governor-cuomo-announces-new-york. (Accessed 15 March 2024).
Amid ongoing COVID-19 pandemic, Governor Cuomo announces NYS on pause functions extended for additional two weeks. Available at: https://www.governor.ny.gov/news/amid-ongoing-covid-19-pandemic-governor-cuomo-announces-nys-pause-functions-extended-additional, (2020)–. (Accessed 15 March 2024).
Anderson, R. M., & May, R. M. (1992). *Infectious diseases of humans: Dynamics and control*. Oxford University Press.
Arthur, R. F., Jones, J. H., Bonds, M. H., Ram, Y., & Feldman, M. W. (2021). Adaptive social contact rates induce complex dynamics during epidemics. *Computational Biology, 17*(2).
ASPE Office of Health Policy. (2022). Impact of the COVID-19 pandemic on the hospital and outpatient clinician workforce. Available at: https://aspe.hhs.gov/sites/default/files/documents/9cc72124abd9ea25d58a22c7692dccb6/aspe-covid-workforce-report.pdf. (Accessed 3 May 2023).
Bansal, S., Grenfall, B. T., & Meyers, L. A. (2007). When individual behaviour matters: Homogeneous and network models in epidemiology. *Journal of the Royal Society, 4*, 879–891.
Berestycki, H., Desjardins, B., Heintz, B., & Plateaus, J. O. (2021). Rebounds and the effects of individual behaviours in epidemics. *Scientific Reports, 11*.
Berestycki, H., Desjardins, B., Weitz, J. S., & Oury, J. M. (2023). Epidemic modeling with heterogeneity and social diffusion. *Journal of Mathematical Biology, 86*(60).
Berman, A., Neumann, M., & Stern, R. J. (1989). *Nonnegative matrices in dynamic systems*. Wiley.
Bir, C., & Widmar, N. O. (2021). Social pressure, altruism, free-riding, and non-compliance in mask wearing by U.S. residents in response to COVID-19 pandemic. *Social Sciences & Humanities Open, 4*(1).
Blower, S. M., & Dowlatabadi, H. (1994). Sensitivity and uncertainty analysis of complex models of disease transmission: An HIV model, as an example. *International Statistical Review, 62*(2), 229–243.
Boserup, B., McKenney, M., & Elkbuli, A. (2020). Alarming trends in US domestic violence during the COVID-19 pandemic. *American Journal of Emergency Medicine, 38*(12).

Bradbury-Jones, C., & Ishlam, L. (2020). The pandemic paradox: The consequences of COVID-19 on domestic violence. *Journal of Clinical Nursing, 29*, 13–14.
Brozak, S. J., Pant, B., Safdar, S., & Gumel, A. B. (2021). Dynamics of COVID-19 pandemic in India and Pakistan: A metapopulation modelling approach. *Infectious Disease Modelling, 6*, 1173–1201.
Carpiano, R. M., Callaghan, T., DiResta, R., Brewer, N. T., Clinton, C., et al. (2023). Confronting the evolution and expansion of anti-vaccine activism in the USA in the COVID-19 era. *The Lancet, 401*(10380), 967–970.
Centers for Disease Control. (2023). COVID-19 outbreak — New York City. Available at: https://www.cdc.gov/mmwr/volumes/69/wr/mm6946a2.htm. (Accessed 15 December 2023).
Centers for Disease Control and Prevention. (2023). Provisional COVID-19 deaths by place of death and state. Available at: https://data.cdc.gov/National-Center-for-Health-Statistics/Provisional-COVID-19-Deaths-by-Place-of-Death-and-/uggs-hy5q/about_data. (Accessed 10 October 2024).
Chen, J., Bhattacharya, P., Hoops, S., Machi, D., Adiga, A., Mortveit, H., et al. (2024). Role of heterogeneity: National scale data-driven agent-based modeling for the US COVID-19 scenario modeling hub. *Epidemics, 48*.
Chin, T., Feehan, D. M., Buckee, C. O., & Mahmud, A. S. (2024). Contact surveys reveal heterogeneities in age-group contributions to SARS-CoV-2 dynamics in the United States. Available at: https://www.medrxiv.org/content/10.1101/2021.09.25.21264082v1.full. (Accessed 30 December 2024).
Cowley, L., Afrad, M. H., Rahman, S. I. A., et al. (2021). Genomics, social media and mobile phone data enable mapping of SARS-CoV-2 lineages to inform health policy in Bangladesh. *Nature Microbiology, 6*(10), 1271–1278.
Cuomo, A. S. (2020). *NYC museums can reopen later this month, bowling alleys on monday*. New York: NBC.
Dai, Y. H. (2002). Convergence properties of the BFGS algoritm. *SIAM Journal on Optimization, 13*(3).
Dan, J. M., & Mateus, J. (2021). Immunological memory to SARS-CoV-2 assessed for up to 8 months after infection. *Science, 371*(6529).
Del Valle, S., Mniszewski, S., & Hyman, J. (2013). Modeling the impact of behavior changes on the spread of pandemic influenza. In *Modeling the interplay between human behavior and the spread of infectious diseases* (pp. 59–77).
Di Marco, G., Hichy, Z., & Sciacca, F. (2021). Attitudes towards lockdown, trust in institutions, and civic engagement: A study on sicilians during the coronavirus lockdown. *Journal of Public Affairs, 22*.
Di Pietro, G. (2023). The impact of COVID-19 on student achievement: Evidence from a recent meta-analysis. *Educational Research Review, 39*, Article 100530.
Eksin, C., Paarporn, K., & Weitz, J. S. (2019). Systematic biases in disease forecasting— the role of behavior change. *Epidemics, 27*, 96–105.
Eksin, C., Shamma, J. S., & Weitz, J. S. (2017). Disease dynamics in a stochastic network game: A little empathy goes a long way in averting outbreaks. *Scientific Reports, 7*(44122).
Espinoza, B., Marathe, M., Swarup, S., & Thakur, M. (2021). Asymptomatic individuals can increase the final epidemic size under adaptive human behavior. *Scientific Reports, 11*.
Espinoza, B., Swarup, S., Barrett, C. L., & Marathe, M. (2022). Heterogeneous adaptive behavioral responses may increase epidemic burden. *Scientific Reports, 12*.
Ezekiel, M. (1930). *Methods of correlation analysis*. Wiley.
Fan, Y., Orhun, A. Y., & Turjeman, D. (2020). *Heterogeneous actions, beliefs, constraints and risk tolerance during the COVID-19 pandemic*.
Farina, L., & Rinaldi, S. (2000). *Positive linear systems: Theory and applications*. Wiley.
Ferrara, E., Cresci, S., & Luceri, L. (2020). Misinformation, manipulation, and abuse on social media in the era of COVID-19. *Computational Social Science, 3*, 271–277.
Ferré-Sadurní, L. (2020). *New York City to close schools, restaurants and bars*. The New York Times. March 15.
Ferwana, I., & Varshney, L. R. (2024). The impact of COVID-19 lockdowns on mental health patient populations in the United States. *Scientific Reports, 14*.
Feuer, A., & Newman, A. (2020). New York City, battered by outbreak, finally moves toward reopening. *The New York Times*.
Funk, S., & Jansen, V. A. A. (2013). The talk of the town: Modelling the spread of information and changes in behaviour. *Modeling the Interplay Between Human Behavior and the Spread of Infectious Diseases*, 93–102.
Gao, S., Pant, B., Williams Chukwu, C., Kwofie, T., Safdar, S., Newman, L., et al. (2023). A mathematical model to assess the impact of testing and isolation compliance on the transmission of COVID-19. *Infectious Disease Modelling, 8*(2), 427–444.
Garad, A., Budiyanto, G., & Al Ansi, A. M. (2021). Impact of COVID-19 pandemic on the global economy and future prospects: A systematic review of global reports. *Journal of Theoretical and Applied Information Technology, 99*(4).
Gmunder, K. N., Ruiz, J. W., Franceschi, D., & Suarez, M. M. (2021). Demographics associated with US healthcare disparities are exacerbated by the tele-medicine surge during the COVID-19 pandemic. *Journal of Telemedicine and Telecare, 30*, 64–71.
M. Gold and L. Ferré-Sadurní. N.Y. gyms and fitness studios can reopen as soon as Aug. 24, Cuomo says. The New York Times, August 17, 2020.
Governor Cuomo announces New York City to enter Phase 1 of reopening on June 8 and five regions enter Phase 2 of reopening today. Available at: https://www.governor.ny.gov/news/governor-cuomo-announces-new-york-city-enter-phase-1-reopening-june-8-and-five-regions-enter::text=Governor, (2020)–. (Accessed 15 March 2024).
Griffin, I., King, J., Lyons, B., Singleton, A. L., Deng, X., & Bruce, B. B. (2024). Estimates ofSARS-CoV-2 hospitalization and fatality rates in the prevaccination period, United States. *Emerging Infectious Diseases*.
Gumel, A. B., Iboi, E. A., Ngonghala, C. N., & Elbasha, E. H. (2021). A primer on using mathematics to understand COVID-19 dynamics: Modeling, analysis and simulations. *Infectious Disease Modelling, 6*, 148–168.
Gumel, A. B., Iboi, E. A., Ngonghala, C. N., & Ngwa, G. A. (2021). Toward achieving a vaccine-derived herd immunity threshold for COVID-19 in the U.S. *Frontiers in Public Health, 9*.
He, D., Dushoff, J., Day, T., Ma, J., & Earn, D. J. D. (2013). Inferring the causes of the three waves of the 1918 influenza pandemic in England and Wales. *Proceedings of the Royal Society B, 280*.
Hethcote, H. W. (2000). The mathematics of infectious diseases. *SIAM Review, 42*(4), 553–786.
J. Jacobs. Museums and other new york cultural institutions can open Aug. 24. The New York Times, August 14, 2020.
Kamgang, J. C., & Sallet, G. (2008). Computation of threshold conditions for epidemiological models and global stability of the disease-free equilibrium (DFE). *Mathematical Biosciences, 213*, 1–12.
Kermack, W. O., & McKendrick, A. G. (1927). A contribution to the mathematical theory of epidemics. *Proceedings of the Royal Society A*.
Kissler, S. M., Tedijanto, C., Goldstein, E., Grad, Y. H., & Lipsitch, M. (2020). Projecting the transmission dynamics of SARS-CoV-2 through the postpandemic period. *Science, 368*(6493), 860–868.
Kitson, J., Costello, I., Chen, J., Hoops, S., Meneses, E., Mortveit, H., et al. (2023). Ten billion events in three minutes: Scaling an agent-based epidemic simulation on realistic social contact networks. Available at: https://www.osti.gov/servlets/purl/2202911. (Accessed 28 December 2024).
Lander, B. (2021). Comptroller Stringer's investigation reveals failures in the city's preparation and response to COVID-19, and outlines recommendations to plan and prepare for future public health emergencies. Available at: https://comptroller.nyc.gov/newsroom/comptroller-stringers-investigation-reveals-failures-in-the-citys-preparation-and-response-to-covid-19-and-outlines-recommendations-to-plan-and-prepare-for-future-public-health-emer/. (Accessed 17 September 2024).
Lauer, S. A., Grantz, K. H., Bi, Q., Jones, F. K., Zheng, Q., et al. (2020). The incubation period of coronavirus disease 2019 (COVID-19) from publicly reported confirmed cases: Estimation and application. *Annals of Internal Medicine*.
LeJeune, L., Ghaffarzadegan, N., Childs, L. M., & Saucedo, O. (2024). Mathematical analysis of simple behavioral epidemic models. *Mathematical Biosciences, 375*.
Li, R., Pei, S., Chen, B., Song, Y., Zhang, T., et al. (2020). Substantial undocumented infection facilitates the rapid dissemination of novel coronavirus (SARS-CoV-2). *Science*.

Lim, T. Y., Xu, R., Ruktanonchai, N., Saucedo, O., Childs, L. M., Jalali, M. S., et al. (2023). Why similar policies resulted in different COVID-19 outcomes: How responsiveness and culture influenced mortality rates. *Global Health Policy, 42*.
Macedo, A., Gonçalves, N., & Febra, C. (2021). COVID-19 fatality rates in hospitalized patients: Systematic review and meta-analysis. *Annals of Epidemiology*.
Marino, S., Hogue, I. B., Ray, C. J., & Kirschner, D. E. (2008). A methodology for performing global uncertainty and sensitivity analysis in systems biology. *Journal of Theoretical Biology, 254*(1), 178–196.
Martecheva, M. (2015). *An introduction to mathematical epidemiology*. New York: Springer.
Martin-Lapoirie, D., D'onofrio, A., Mccoll, K., & Raude, J. (2023). Testing a simple and frugal model of health protective behaviour in epidemic times. *Epidemics, 42*.
McLeod, R. G., Brewster, J. F., Gumel, A. B., & Slonowsky, D. A. (2006). Sensitivity and uncertainty analyses for a SARS model with time-varying inputs and outputs. *Mathematical Biosciences and Engineering, 3*(3), 527–544.
McNeil, D. G. (2020). Mask hoarders may raise risk of a coronavirus outbreak in the U.S.. Available at: https://www.nytimes.com/2020/01/29/health/coronavirus-masks-hoarding.html. (Accessed 29 January 2020).
Mian, A., & Khan, S. (2020). Coronavirus: The spread of misinformation. *BMC Medicine, 18*(89).
Moghadas, S. M., Fitzpatrick, M. C., Sah, P., Pandey, A., Shoukat, A., Singer, B. H., et al. (2020). The implications of silent transmission for the control of COVID-19 outbreaks. *PNAS, 117*(30).
MTA subway and bus mask compliance statistics: 2020–2022. Available at: https://data.ny.gov/Transportation/MTA-Subway-and-Bus-Mask-Compliance-Statistics-2020/ijxr-nffj/about_data, (2024)–. (Accessed 11 December 2024).
Munoz-Fernandez, G. A., Seoane, J. M., & Seoane-Sepulveda, J. B. (2021). A SIR-type model describing the successive waves of COVID-19. Chaos. *Solitons and Fractals, 144*.
Naseer, S., Khalid, S., Parveen, S., Abbass, K., & Song, H. (2022). COVID-19 outbreak: Impact on global economy. *Frontiers in Public Health, 10*.
Newman, A. (2020). *Are new yorkers wearing masks? Here's what we found in each borough*. The New York Times. August 20.
Ngonghala, C. N., Iboi, E., Eikenberry, S., Scotch, M., MacIntyre, C. R., et al. (2020). Mathematical assessment of the impact of non-pharmaceutical interventions on curtailing the 2019 novel coronavirus. *Mathematical Biosciences, 325*.
Ngonghala, C. N., Iboi, E. A., & Gumel, A. B. (2020). Could masks curtail the post-lockdown resurgence of COVID-19 in the us? *Mathematical Biosciences, 329*.
Ngonghala, C. N., Knitter, J. R., Marinacci, L., Bonds, M. H., & Gumel, A. B. (2021). Assessing the impact of widespread respirator use in curtailing COVID-19 transmission in the USA. *Open Science, 8*.
Nguyen, M. M., Freedman, A. S., Cheung, M. A., Saad-Roy, C. M., Espinoza, B., Grenfell, B. T., et al. (2024). The complex interplay between risk tolerance and the spread of infectious diseases. Available at: https://www.medrxiv.org/content/10.1101/2024.07.01.24309771v1. (Accessed 18 July 2024).
Nishiura, H., Kobayashi, T., Miyama, T., Suzuki, A., Jung, S., Hayashi, K., et al. (2020). Estimation of the asymptomatic ratio of novel coronavirus infections (COVID-19). *International Journal of Infectious Diseases, 94*, 154–155.
NYC Health. COVID-19 data. Available at: https://www.nyc.gov/site/doh/covid/covid-19-data-totals, (2023)–. (Accessed 15 December 2023).
Ochab, M., Manfredi, P., Puszynski, K., & d'Onofrio, A. (2023). Multiple epidemic waves as the outcome of stochastic SIR epidemics with behavioral responses: A hybrid modeling approach. *Nonlinear Dynamics*.
Panchal, U., de Pablo, G. S., Franco, M., Moreno, C., Parellada, M., et al. (2023). The impact of COVID-19 lockdown on child and adolescent mental health: Systematic review. *European Child & Adolescent Psychiatry, 32*, 1151–1177.
Pant, B., & Gumel, A. B. (2024). Mathematical assessment of the roles of age heterogeneity and vaccination on the dynamics and control of SARS-CoV-2. *Infectious Disease Modelling, 9*.
Pant, B., Safdar, S., Santillana, M., & Gumel, A. B. (2024). Mathematical assessment of the role of human behavior changes onSARS-CoV-2 transmission dynamics in the United States. *Bulletin of Mathematical Biology, 86*.
Parady, G., Taniguchi, A., & Takami, K. (2020). Travel behavior changes during the COVID-19 pandemic in Japan: Analyzing the effects of risk perception and social influence on going-out self-restriction. *Transportation Research Interdisciplinary Perspectives, 7*.
Pathak, E. B., Garcia, R. B., Menard, J. M., & Salemi, J. L. (2021). Out-of-hospital COVID-19 deaths: Consequences for quality of medical care and accuracy of cause of death coding. *American Journal of Public Health, 111*.
Pei, L., & Zhang, M. (2022). Long-term predictions of current confirmed and dead cases of COVID-19 in China by the non-autonomous delayed epidemic models. *Cognitive Neurodynamics, 16*.
Pisaneschi, G., Tarani, M., Di Donato, G., Landi, A., Laurino, M., & Manfredi, P. (2024). Optimal social distancing in epidemic control: Cost prioritization, adherence and insights into preparedness principles. *Scientific Reports, 14*.
Qiu, Z., Espinoza, B., Vasconcelos, V. V., Chen, C., Constantino, S. M., Crabtree, S. A., et al. (2022). Understanding the coevolution of mask wearing and epidemics: A network perspective. *PNAS, 119*.
Saad-Roy, C. M., & Traulsen, A. (2023). Dynamics in a behavioral–epidemiological model for individual adherence to a nonpharmaceutical intervention. *PNAS, 120*(44).
Scandurra, C., Bochicchio, V., Dolce, P., Valerio, P., Muzii, B., et al. (2023). Why people were less compliant with public health regulations during the second wave of the COVID-19 outbreak: The role of trust in governmental organizations, future anxiety, fatigue, and COVID-19 risk perception. *Current Psychology, 42*.
Sediri, S., Zgueb, Y., Ouanes, S., Ouali, U., Bourgou, S., et al. (2020). Women's mental health: Acute impact of COVID-19 pandemic on domestic violence. *Archives of Women's Mental Health, 23*, 749–756.
Sharbayta, S. S., Buonomo, B., d'Onofrio, A., & Abdi, T. (2022). 'Period doubling' induced by optimal control in a behavioral SIR epidemic model. *Chaos, Solitons & Fractals, 161*.
Shin, S. H., Ji, H., & Lim, H. (2021). Heterogeneity in preventive behaviors during COVID-19: Health risk, economic insecurity, and slanted information. *Social Science & Medicine, 278*.
Smith, R. J., Bodine, E. N., Wilson, D. P., & Blower, S. M. (2005). Evaluating the potential impact of vaginal microbicides to reduce the risk of acquiring HIV in female sex workers. *AIDS, 19*(4), 413–421.
Stoler, J. (2022). Sociopolitical and psychological correlates of COVID-19 vaccine hesitancy in the United States during Summer 2021. *Social Science & Medicine, 306*.
Strogatz, S. H. (2024). Nonlinear dynamics and chaos. In *Third edition: With applications to physics, biology, chemistry and engineering*. Chapman and Hall.
Sy, K. T. L., White, L. F., & Nichols, B. E. (2021). Population density and basic reproductive number of COVID-19 across United States counties. *PLoS One, 16*(4).
Tang, K. H. D. (2022). Impacts of COVID-19 on primary, secondary and tertiary education: A comprehensive review and recommendations for educational practices. *Educational Research for Policy and Practice, 22*, 23–61.
Tang, B., Bragazzi, N. L., Li, Q., Tang, S., Xiao, Y., et al. (2020). An updated estimation of the risk of transmission of the novel coronavirus (2019-nCoV). *Infectious Disease Modelling*.
United States Bureau of Labor Statistics. (2024). Industries at a glance— hospitals: Naics 622. Available at: https://www.bls.gov/iag/tgs/iag622.htm. (Accessed 25 April 2024).
Uscinski, J. (2022). Cause and effect: On the antecedents and consequences of conspiracy theory beliefs. *Current Opinion in Psychology, 47*.
Venkatramanan, S., Cambeiro, J., Liptay, T., Lewis, B., Orr, M., Dempsey, G., et al. (2022). Utility of human judgment ensembles during times of pandemic uncertainty: A case study during the COVID-19 omicron BA.1 wave in the USA. Available at: https://www.medrxiv.org/content/10.1101/2022.10.12.22280997v1. (Accessed 18 July 2024).
Verplanken, B., & Orbell, S. (2022). Attitudes, habits, and behavior change. *Annual Review of Psychology, 73*.
Viskupic, F., & Wiltse, D. L. (2022). The messenger matters: Religious leaders and overcoming COVID-19 vaccine hesitancy. *Political Science and Politics, 55*(3).
Waites, C. P. W. (2022). Transmission dynamics of SARS-CoV-2 in a strictly-Orthodox Jewish community in the UK. *Scientific Reports, 12*.

Walmsley, T., Rose, A., John, R., Wei, D., Hlávka, J. P., et al. (2023). Macroeconomic consequences of the COVID-19 pandemic. *Economic Modelling, 120*.
Weitz, J. S., Park, S. W., Eksine, C., & Dushoff, J. (2020). Awareness-driven behavior changes can shift the shape of epidemics away from peaks and toward plateaus, shoulders, and oscillations. *PNAS, 117*(51), 32764–32771.
World Health Organization. (2023). WHO coronavirus dashboard. Available at: https://covid19.who.int/. (Accessed 31 October 2023).
Yang, L., Constantino, S. M., Grenfell, B. T., Weber, E. U., Levin, S. A., & Vasconcelos, V. V. (2022). Sociocultural determinants of global mask-wearing behavior. *PNAS, 119*(41).
Yue, T., Fan, B., Zhao, Y., Wilson, J. P., Du, Z., et al. (2021). Dynamics of the COVID-19 basic reproduction numbers in different countries. *Scientific Bulletin, 66*(3), 229–232.
Zhai, Y., & Han, G. (2023). Lockdown, information quality, and political trust: An empirical study of the Shanghai lockdown under COVID-19. *International Review of Administrative Sciences, 90*.